Department of Physics and Astronomy
University of Heidelberg

Bachelor Thesis in Physics
submitted by

Sophia Dorra

born in Frankfurt am Main (Germany)

2023

Few-Level Model and RABITT

This Bachelor Thesis has been carried out by
Sophia Dorra
at the Max-Planck Institut für Kernphysik in Heidelberg
under the supervision of
Prof. Dr Robert Moshammer, Prof. Dr. Anne Harth and Divya Bharti

Abstract

This thesis investigates the interaction of an atom (described by discrete energy levels) with an electric field $E(t)$ using the few-level model. First, a 2-level system is discussed, whereby a distinction is made between the interaction with a continuous electric field and with a time-limited electric field, defined by a pulse with a pulse area $A(t)$. Two different methods were used and compared to determine the population of the ground state and the excited state: the analytical method utilizing the Rotating-Wave Approximation and a Numerical method using the Runge-Kutta Method. In addition, multiphoton transitions and 2-level systems with decay are considered. Then the same process is applied to a 5-level system and its effect is examined. Finally, consider the application of the few-level model to RABITT.

Zusammenfassung

Diese Arbeit untersucht mithilfe des Few-Level Model die Wechselwirkung eines Atoms (beschrieben durch diskrete Energieniveaus) mit einem elektrischen Feld $E(t)$. Dabei wird zuerst auf ein 2-Level System eingegangen, wobei dort unterschieden wird von der Wechselwirkung zum einen mit einem kontinuierlichen elektrischen Feld und zum anderen mit einem zeitlich beschränkten elektrischen Feld, definiert durch einen Puls mit Pulsbereich $A(t)$. Zur Bestimmung der Population von Grundzustand und dem anegregten Zustand wurden zwei verscheidene Methoden angewandt und verglichen: die analytische Methode unter Verwendung der Drehwellennäherung und eine numerische Methode unter Verwendung der Runge-Kutta-Methode. Außerdem werden Multiphoton-Übergänge und 2-Level Systeme mit Verfall betrachtet. Anschließend wird der selbe Prozess angewandt auf ein 5-Level System und dessen Wirkung wird untersucht. Zum Schluss betrachte man die Anwendung des Few-Level Models an RABITT.

Contents

1 Introduction

The introduction of RABBITT originated in the temporal characterization of attosecond pulse trains (APTs) by reconstructing attosecond oscillations by interference of two-photon transitions [20, 21]. The APTs are generated by harmonic generation (HHG). In the meantime, RABBITT is exclusively used to study the attosecond dynamics in atoms, molecules and solids [22–25].
For further testing and investigation with the RABBITT technique, it is advantageous to use a simple model for simulating RABBITT. The few-level model offers one possibility.

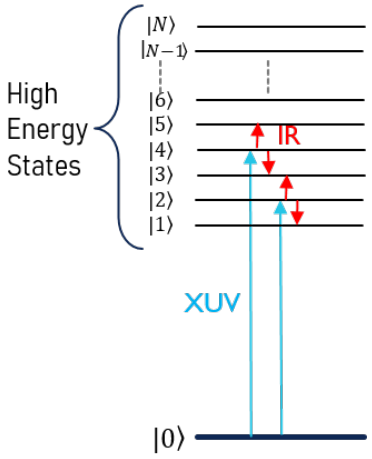

Figure 1: Few-Level Model: Interaction of an XUV-pulse (ultraviolet pump pulse) and an IR-pulse (infrared probe pulses) with a few-level system, where the XUV-pulse couples the ground state to the higher energy states and the IR-pulse redistributes the population within the higher energy states.

The main goal of this thesis is to test and simulate RABBITT with a Few-Level Model. For this, first consider the simplest model, namely the 2-level model (a two-level atom) for fundamental investigations. First, two different methods, the rotating wave approximation and the Runge-Kutta method, are compared to determine the population probability of the ground state and the upper state. This is for the purpose of assessing which methods are best suited for determining the population probability of energy levels, which is also crucial for its application to RABBIT. Furthermore, multiphoton transitions and a two-level system with delay are investigated. This is for motivation to simulate RABBITT with a delay.

In the next chapter a 5-level system is dealt with, mainly to study the population probability of several energy levels, but also to study a compression of the upper energy levels. This serves the purpose of getting an insight into the simulation of a continuous upper state. For RABBITT there is the possibility to approximate the upper energy states to a continuum state by adding a larger number of closely spaced energy levels near the resonance states.

In the final chapter, some of the information gathered from the previous chapter is applied to RABBITT by the few-level model. In addition, the effects of applying an XUV pulse with and without chirp are examined.

2 Theoretical Background

This section covers some theoretical aspects on light-matter interaction. It starts with an introduction to Ultrashort pulses, before it turns to the fundamentals of quantum dynamics. The Few-Level model is briefly discussed. Throughout this thesis all calculations, simulations and numerical experiments are done using SI-units.

2.1 Ultrashort pulses of light

Maxwell's theory of electromagnetic light propagation revolves around the wave characteristics of light. A space- and time-dependent electric field $\mathbf{E}(\mathbf{x}, t)$ contains all information to fully describe such electromagnetic radiation. When regarding invariant, linearly polarized light, the vectorial and spatial properties can be omitted and the electric field reduces to a scalar quantity $E(t)$.
Since short light pulses are characterized by a continuum of frequencies, we can give an alternate representation in the frequency domain by using Fourier's theorem:

$$\tilde{E}(\omega) = \frac{1}{\sqrt{2\pi}} \int_{-\infty}^{\infty} E(t) e^{i\omega t} dt. \tag{1}$$

The function $\tilde{E}(\omega)$ is complex-valued, denoted by the tilde and can be called spectral field. By applying the inverse Fourier transform, the real-valued electric field can be regained:

$$E(t) = \frac{1}{\sqrt{2\pi}} \int_{-\infty}^{\infty} \tilde{E}(\omega) e^{i\omega t} d\omega. \tag{2}$$

The spectral field is symmetric around $\omega = 0$ and can generally be written in terms of an amplitude and phase:

$$\tilde{E}(\omega) = \tilde{\mathcal{E}}(\omega) e^{i\tilde{\phi}(\omega)}. \tag{3}$$

The spectral phase $\tilde{\phi}(\omega)$ is defined in the frequency domain and can be expanded as a power series into:

$$\tilde{\phi}(\omega) = \phi_0 + \tau(\omega - \omega_0) + b(\omega - \omega_0)^2 + c(\omega - \omega_0)^3 + \dots \tag{4}$$

Here ϕ_0 describes a constant offset and τ is called the group delay (gd) which causes a temporal shift of the pulse. The second-order phase term b is known as the group-delay dispersion (gdd) and causes a linear chirp of the pulse. Higher order terms are simply referred to as third order dispersion (TOD) and so on.
Further mathematical descriptions of ultra short pulses of light can be found in text books [1]. In this thesis higher order dispersion effects of $n \geq 4$ are disregarded, since their effects on the pulse shape are minimal.

2.2 Quantum dynamics

In non-relativistic quantum mechanics the most fundamental description of a time-dependent quantum system is given by the Schrödinger equation:

$$-i\frac{\partial}{\partial t}\left|\psi(x,t)\right\rangle = \mathcal{H}(t)\left|\psi(x,t)\right\rangle . \tag{5}$$

Here, $|\psi(x,t)\rangle$ corresponds to a time-dependent wave function and $\mathcal{H}(t)$ denotes the Hamiltonian describing the system. In a stationary system with time-independent Hamiltion $\mathcal{H}$, equation (5) becomes an eigenvalue equation:

$$\mathcal{H}\left|\psi_k\right\rangle = E_k\left|\psi_k\right\rangle , \tag{6}$$

where $|\psi_k\rangle$ constitutes a set of orthogonal eigenstates, each associated with an energy E_k. The first energy level E_1 corresponds to the ground state of the system. By representing a state as a superposition of eigenstates, a general solution of the Schrödinger equation can be given by:

$$\left|\psi(x,t)\right\rangle = \sum_{k=1}^{n} c_k(t)\left|\psi_k(x,t)\right\rangle . \tag{7}$$

The absolute squares of the coefficients $c_i = \langle\psi_i|\psi\rangle$ sum up to 1 ($\sum_{i=0}^{n}|c_i|^2 = 1$), if the normalization is given, since the physical interpretation of the expansion coefficients is the probability to find the considered system in a state $|\psi_k\rangle$. For given initial conditions, the time propagation of a general state (equation (7)) is a phase evolution:

$$\left|\psi(x,t)\right\rangle = \sum_{n} e^{-iE_n t/\hbar} c_n(t)\left|\psi_n(x)\right\rangle . \tag{8}$$

2.3 Few-Level-Model

For the study of quantum systems deemed too complicated for analytical solutions, numerical simulations can help to provide insights into the inner dynamics of such a system. To implement simulations, one must first conceptualize models that describe the major features of a quantum system. The following sections are intended to act as an introduction to the basic concepts of a Few-Level Model and its numerical solution.
For studies regarding the dynamics of light-matter interactions such as ultrashort laser pulses in simple quantum systems, it is advantageous to separate the total Hamiltonian $\mathcal{H}$ into two parts:

$$\mathcal{H}(t) = \mathcal{H}_0 + \mathcal{H}_{int}(t). \tag{9}$$

The first operator $\mathcal{H}_0$ describes an unperturbed, time-independent system, whereas $\mathcal{H}_{int}$ denotes the light-matter interacting part of the system. Since all systems we consider can be described by a finite number of states, we can expand the wave function into a finite set of energy eigenstates of the unperturbed system:

$$|\psi(t)\rangle = \sum_{k=1}^{n} c_k(t) \, |k\rangle \, , \tag{10}$$

where $c_k(t)$ are complex-valued, time-dependent state coefficients. The time evolution of such a system can be found by expressing the state in its eigenbasis. By projecting $\langle\psi(t)|$ onto $|\psi\rangle$, we can depict the Hamiltonian by a $n \times n$ matrix, with energies $E_k = \langle k| \, \mathcal{H}_0 \, |k\rangle$ on the diagonal and couplings between states $D_{kl} = \langle k| \, \mathcal{H}_{int}(t) \, |l\rangle$ on the off-diagonal:

$$\mathcal{H} = \begin{pmatrix} E_1 & D_{12} & \dots & D_{1n} \\ D_{21} & E_2 & & D_{2n} \\ \vdots & & \ddots & \vdots \\ D_{n1} & D_{n2} & \dots & E_n \end{pmatrix}, \qquad |\psi\rangle = \begin{pmatrix} c_1(t) \\ c_2(t) \\ \vdots \\ c_n(t) \end{pmatrix}. \tag{11}$$

Using dipole approximation, the interacting part can be described by $\mathcal{H}_{int} = \hat{d} \cdot E(t)$, where $\hat{d}$ and $E(t)$ represent the dipole moment and the electric field. Therefore the matrix elements D_{kl} can be evaluated as:

$$D_{kl} = \langle k| \, \mathcal{H}_{int}(t) \, |l\rangle = \langle k| \, \hat{d} \, |l\rangle \cdot E(t). \tag{12}$$

A formal solution for the Schrödinger equation implementing (52) is:

$$|\psi(t)\rangle = e^{-i\mathcal{H}t} \, |\psi_0\rangle \, , \tag{13}$$

with $|\psi_0\rangle = |\psi(t=0)\rangle$ representing the initial wavefunction.

3 Two-Level Model

3.1 Atom-Light Interaction: Two-Level Approximation

The Two-level model, to represent the coupling of a 2-level atom, is the simplest model to reveal the essential features of interactions [2–6]. In the standard semi-classical version, in which the field is treated as a purely classical electric field, the atom's probabilities of being in the ground state or excited state differ with time [7–13]. The Two-level atom experiences optical Rabi oscillations at Rabi-Frequency between ground state and excited state under the action of the driving electromagnetic field.

The Rotating-Wave Approximation is a fundamental and important approximation used in atomic optics [14–16] and magnetic resonance. The approximation is only applicable when the excitation frequency (electric field) is close to the resonance frequency of the two states [17–19].

3.1.1 The analytical solution with Rotating-Wave Approximation

In Figure 2 consider the interaction of a two-level atom with an electric field of frequency ω_0. Let $|g\rangle$ and $|e\rangle$ represent the ground and upper states of the atom, they are eigenstates of the unperturbed part of the Hamiltonian H_0 with the eigenvalues $E_g = \hbar\omega_g$ and $E_e = \hbar\omega_e$, respectively, and ω_{eg} is the transition frequency of the two levels.

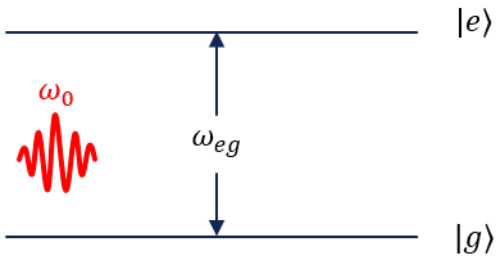

Figure 2: Two-Level Model: Photon transition with an Energy of $E_{ph} = \omega_0 \cdot \hbar/e = 1.5\ eV$ between the ground state and upper state.

The incident electric field with initial phase φ and amplitude E_0 to interact with the atom can be expressed as

$$E(t) = E_0 \cos(\omega_0 t + \varphi). \tag{14}$$

According to (7), the wave function of a two-level atom can be written in the form

$$|\psi(t)\rangle = C_g(t)\,|g\rangle + C_e(t)\,|e\rangle\,, \tag{15}$$

where C_g and C_e are the probability amplitudes of the two levels, respectively. For the corresponding Schrödinger equation, accordingly to (5), the Hamiltonian is given by

$$\mathcal{H} = \mathcal{H}_0 + \mathcal{H}_{int}, \tag{16}$$

where $\mathcal{H}_0$ and $\mathcal{H}_{int}$ represent the unperturbed and interaction Hamiltonian, respectively. We can write $\mathcal{H}_0$ and H_{int} as

$$\mathcal{H} = \hbar\omega_g \left|g\right\rangle \left\langle g\right| + \hbar\omega_e \left|e\right\rangle \left\langle e\right|, \tag{17}$$

and

$$\mathcal{H}_{int} = -(D_{ge} \left|g\right\rangle \left\langle e\right| + D_{eg} \left|e\right\rangle \left\langle g\right|)E(t), \tag{18}$$

respectively, and $D_{eg} = D_{ge}^*$ is the dipole matrix element. In order to solve for C_g and C_b, we first write $C_g = c_g \exp(-i\omega_g t)$ and $C_e = c_e \exp(-i\omega_e t)$, where c_g and c_e are the slowly varying probability amplitude. In the dipole approximation, the equations of motion for c_g and c_e may be written as

$$\dot{c_g}(t) = i\Omega_R c_e \frac{\exp\left(-i\Delta t + i\varphi\right) + \exp\left(-i[\omega_{eg} + \omega_0]t - i\varphi\right)}{2}, \tag{19}$$

$$\dot{c_e}(t) = i\Omega_R c_g \frac{\exp\left(i\Delta t - i\varphi\right) + \exp\left(i[\omega_{eg} + \omega_0]t + i\varphi\right)}{2}, \tag{20}$$

where $\Delta = \omega_{eg} - \omega$ is the detuning between field and atomic resonance and the Rabi frequency Ω_R is defined as

$$\Omega_R = \frac{|D_{eg}|E_0}{\hbar}, \tag{21}$$

and $\omega_{eg} = \omega_e - \omega_g = \omega_{ge} > 0$ is the atomic transition frequency. To solve the equations, we divide them into two terms which are approximate co-rotating terms proportional to $\exp\left(\pm i\Delta\right)$ and counter-rotating terms proportional to $\exp\left(\pm i[\omega_{eg} + \omega]\right)$. Influences of rapidly rotating terms in the Hamiltonian of a system are neglected so we only are going to focus on the co-rotating terms, which corresponds to the Rotating-Wave Approximation (RWA). This method is generally a very good approximation for resonant or weakly detuned situations. Then the equations turn into

$$\dot{c_g}(t) = i\Omega_R c_e \frac{\exp\left(-i\Delta t + i\varphi\right)}{2}, \tag{22}$$

$$\dot{c_e}(t) = i\Omega_R c_g \frac{\exp\left(i\Delta t - i\varphi\right)}{2}. \tag{23}$$

One assumes that the Two-Level System is initially in the state $|g\rangle$, therefore $c_g(0) = 1$, $c_e(0) = 0$. Using the abbreviation

$$\Omega_\Delta = \sqrt{\Delta^2 + \Omega_R^2}, \tag{24}$$

the solution of amplitude of the upper level state can be written as

$$c_e(t) = i\frac{\Omega_R}{\Omega_\Delta} c_g \exp\left(i\Delta t/2\right) \sin\left(t \cdot \Omega_\Delta/2\right). \tag{25}$$

The probabilities of the atom being in states $|g\rangle$ and $|e\rangle$ at time t are then given by $|c_g(t)|^2$ and $|c_e(t)|^2$, and the probability of finding the atom in the upper level state is

$$|c_e(t)|^2 = c_e c_e^* = (\frac{\Omega_R}{\Omega_\Delta})^2 \sin^2\left(t \cdot \Omega_\Delta/2\right) \tag{26}$$

(26) indicates the probability is a periodic function of time and the total population probability remains 1, therefore

$$|c_g(t)|^2 = 1 - |c_e(t)|^2 = (\frac{\Omega_R}{\Omega_\Delta})^2 \cos^2\left(t \cdot \Omega_\Delta/2\right). \tag{27}$$

One can see that the system oscillates with the frequency of Ω_Δ between the two atomic levels. Ω_R relies on the detuning $\Delta = \omega_{eg} - \omega_0$, the amplitude of field E_0 and the dipole matrix element D_{ge}. In the special case when the atom is in resonance with the incident optical field ($\Delta = \omega_{eg} - \omega_0 = 0$), one gets $\Omega_R = \Omega_\Delta$, so (26) and (27) transform into

$$|c_g(t)|^2 = \cos^2(t \cdot \Omega_R/2) \tag{28}$$

and

$$|c_e(t)|^2 = \sin^2(t \cdot \Omega_R/2) \tag{29}$$

Now begin to examine the Rotating-Wave Approximation by plotting the population probability of the two atomic states.
For this assume a photon energy of $E_{ph} = \omega_0 \cdot \hbar/e = 1.5\ eV$, a dipole coupling element of $|D_{eg}| = 0.5 \cdot 10^{-28}\ Cm$, an intensity of the continuous electric field $E_0 = 22 \cdot 10^8\ V/m$ and the initial conditions $c_g(0) = 1$ and $c_e(0) = 0$ for all following investigations on the Two-Level system.

In the following figure, the population probability of the ground state and the upper energy state is plotted against $t \cdot \Omega_R$. The course of the population probability corresponds to equations (28) and (29) since the detuning $\Delta = 0$. Consider the interaction of a two-level atomic system with a continuous electric field $E(t)$, as shwon in fig. 2.

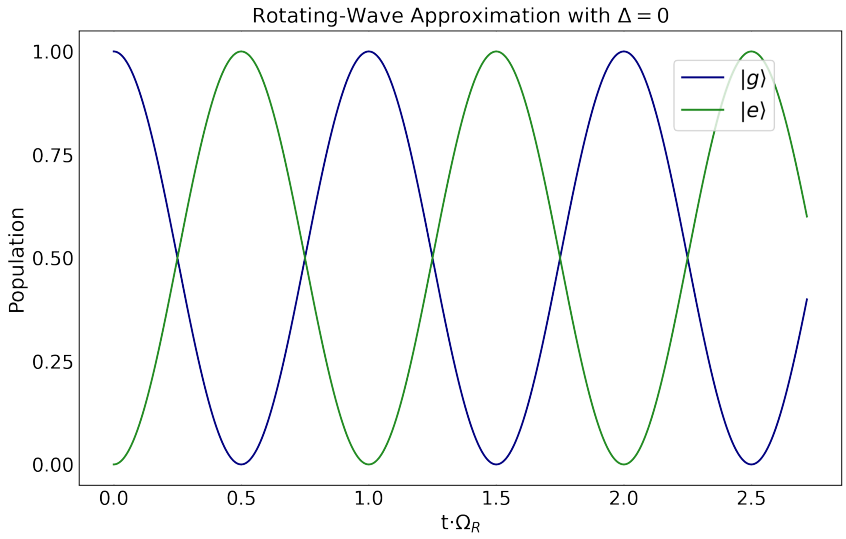

Figure 3: The Population of the ground state $|g\rangle$ and the upper state $|e\rangle$ (computed with the Rotating-Wave Approximation), with the detuning $\Delta = 0$.

A phase shift of π between the two population curves can be seen, and accordingly a continuous excitation of the upper energy state takes place.
The ground state is completely occupied at the beginning, whereas the upper energy state is not

populated. After the arrival of the electric field $E(t)$, photon-absorption and -emission occur, causing the occupation of the two energy states to oscillate, namely with the Rabi frequency Ω_R. This is the case because in Figure 4 the excitation frequency ω_0 is equal to the resonance frequency ω_{eg} and thus $\Delta = 0$.

Now consider the population probability of the two states with small differences between the resonance frequency ω_{eg} and the excitation frequency ω_0, which corresponds to increasing the detuning Δ.

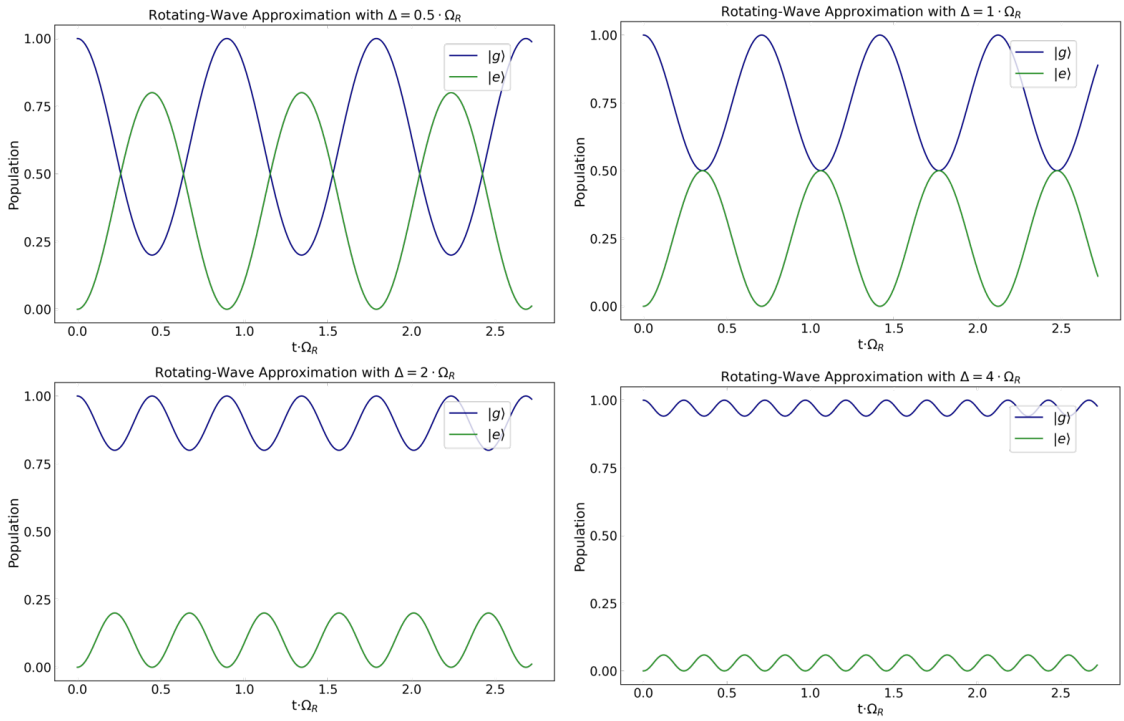

Figure 4: The Population of the ground state $|g\rangle$ and the upper state $|e\rangle$ (computed with the Rotating-Wave Approximation) at different detunings Δ.

Firstly, Figure 4 shows that the probability of occupying the upper energy level decreases with a higher detuning Δ. Secondly, the Rotating-Wave Approximation is satisfied just for near-resonance situation, because only in this case, the counter-rotating terms can be ignored. When the detuning is $\Delta >> 0$, the approximation is no longer applicable. In the figure above, the detuning of Δ is still very small, but in the next section you can already see another oscillation when considering the rapidly rotating terms. However, only the Rabi oscillation seems to be visible for the Rotating-Wave Approximation, but further investigations are carried out in the following sections.

In the appendix you can find further representation of the population probability of the two states for other detunings Δ.

Now consider another figure representing the Rabi cycle by considering the population probability for the upper state at two different detunings Δ.

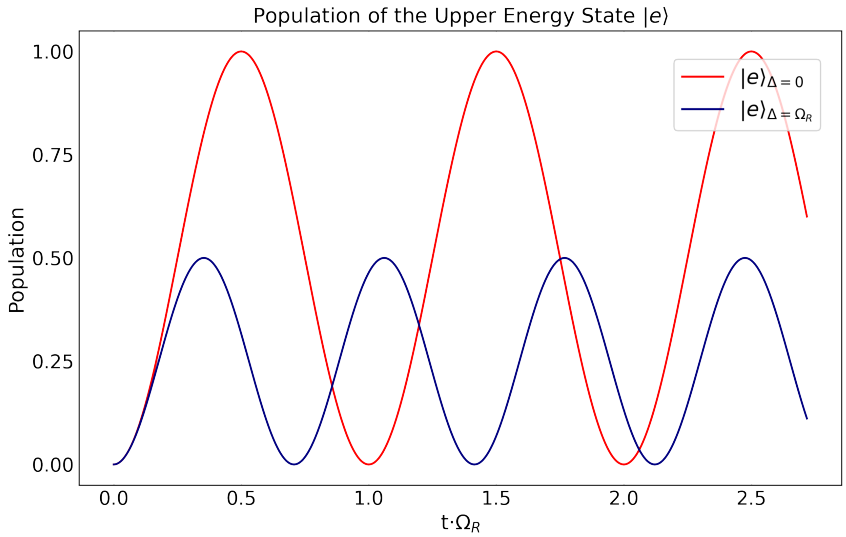

Figure 5: The influence of Rabi oscillation on the upper energy level population (computed with the Rotating-Wave Approximation): A comparison of the occupation progression with $\Delta = 0$ (marked in red) and $\Delta = \Omega_R$ (marked in blue).

The continuous arrival of photons, caused by the electric field $E(t)$, causes a cyclic absorption and emission (stimulated emission) of photons. This cycle is called Rabi cycle or Rabi flop.

If you look at the population at the point $t \cdot \Omega_R = 1$ in Figure 6, you can see that for $\Delta = 0$ the 2-level system is again in the initial state, but for $\Delta = \Omega_R$ the system is in a superposition of $|g\rangle$ and $|e\rangle$. Accordingly, the detuning Δ has an impact on the probability that a state change will take place in the system.

3.1.2 The numerical solution with Runge-Kutta Method

The counter-rotating terms are more significant the larger the detuning ($\Delta >> 0$) becomes and the Runge-Kutta Method (RK4) gives a way to solve the equations of motion for c_g (19) and c_e (20) without ignoring the counter-rotating terms.

The initial value problem is specified as

$$\frac{dc}{dt} = f(t, c), \qquad c_g(t_0) \widehat{=} c_0(t_0) = 1 \text{ and } c_e(t_0) \widehat{=} c_1(t_0) = 0 \tag{30}$$

with

$$f(t, c_g) = i\Omega_{ge} c_e \frac{\exp\left(-i\Delta t + i\varphi\right) + \exp\left(-i[\omega_{eg} + \omega]t - i\varphi\right)}{2} \tag{31}$$

$$f(t, c_e) = i\Omega_{ge} c_g \frac{\exp\left(-i\Delta t - i\varphi\right) + \exp\left(-i[\omega_{eg} + \omega]t + i\varphi\right)}{2} \tag{32}$$

where $c(t)$ defines the slowly varying probability amplitude. The rate at which c changes, is a function of time t and of c itself. The function f and the initial conditions t_0 and c_0 are given.

Now you pick a step-size $h > 0$ (in this thesis $h = 10 \cdot 10^{-3}\ fs$) and for $n \in \mathbf{N}$ define:

$$\begin{aligned} c_{n+1} &= c_n + \frac{1}{6}(k_1 + 2k_2 + 2k_3 + k_4), \\ t_{n+1} &= t_n + h \end{aligned} \tag{33}$$

and

$$\begin{aligned} k_1 &= f(t_n, c_n), \\ k_2 &= f(t_n + \frac{h}{2}, c_n + h\frac{k_1}{2}), \\ k_2 &= f(t_n + \frac{h}{2}, c_n + h\frac{k_1}{2}), \\ k_3 &= f(t_n + \frac{h}{2}, c_n + h\frac{k_2}{2}), \\ k_4 &= f(t_n + h, c_n + hk_3). \end{aligned} \tag{34}$$

The population of the ground state and the upper energy state were plotted using the Runge-Kutta method, first at a detuning $\Delta = 0$.

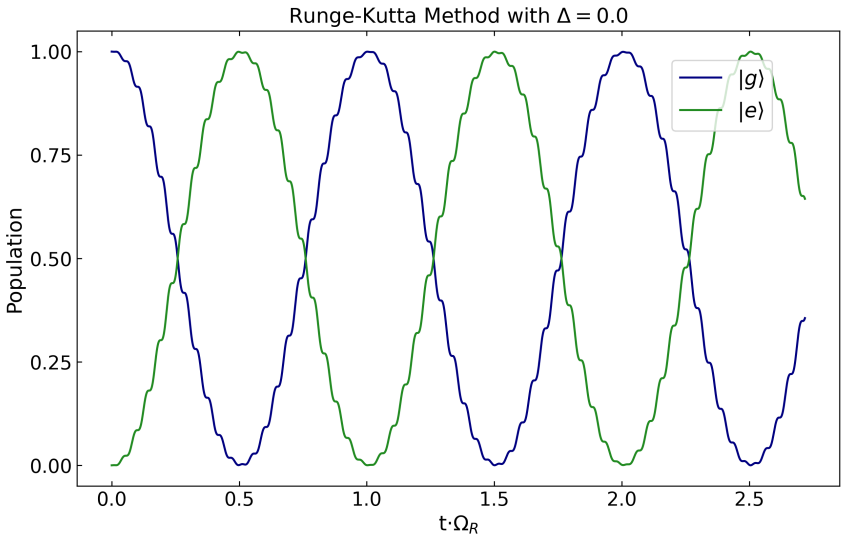

Figure 6: The Population of the ground state $|g\rangle$ and the upper state $|e\rangle$ (computed with the Runge-Kutta Method), with the detuning $\Delta = 0$.

The course of the population probability of the two states is also cyclical, as in Figure 3, and a phase shift of π between the two population curves can be seen.
However, unlike the Rotating-Wave Approximation, another oscillation can be seen. The counter-rotating terms are neglected in the Rotating-Wave Approximation, which is not the case in the Runge-Kutta method. An assumption for this oscillation is therefore the influence of the counter-rotating terms, more details will be given in the next section (3.1.3).

In the next figure, the population of the two energy states at different detunings is shown.

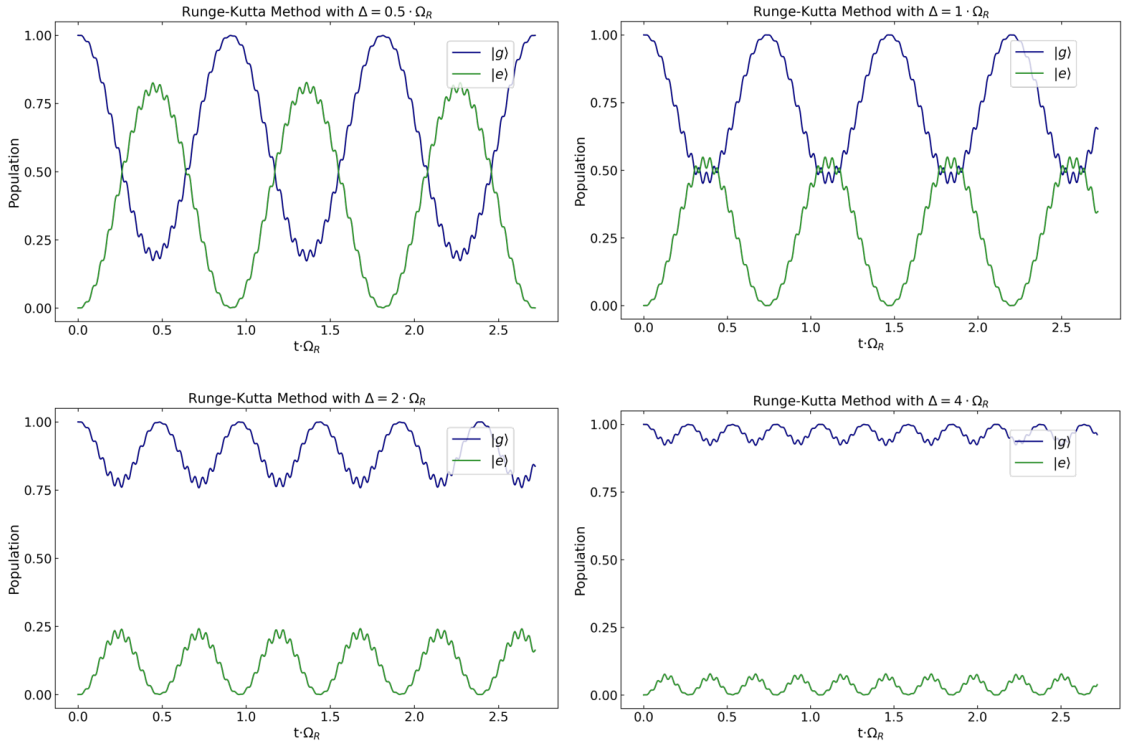

Figure 7: The Population of the ground state $|g\rangle$ and the upper state $|e\rangle$ (computed with the Runge-Kutta Method) at different detunings Δ.

The probability that the upper energy state is occupied or that the system is in an excited state is reduced by the greater the detuning Δ is. In contrast to Figure 4, the respective population peaks are more significant, caused by the oscillation of the counter-rotating terms. This is especially noticeable at $\Delta = \Omega_R$, where the population peaks overlap, although there is hardly any contact of the population peaks in the case of the Rotating-Wave Approximation (Fig. 4). Increasing the excitation frequency ω_0 (and increase proportional to that the resonance frequency ω_{eg}) causes a decrease in the influence of the counter-rotating terms, which dampens the oscillation and brings the population curves closer to the representation in Figure 5. An example can be found in the appendix.

n the appendix you can find further representation of the population probability (computed with the Runge-Kutta method) of the two states for other detunings .

A representation of the Rabi cycle or Rabi flop is also shown in Figure 8:

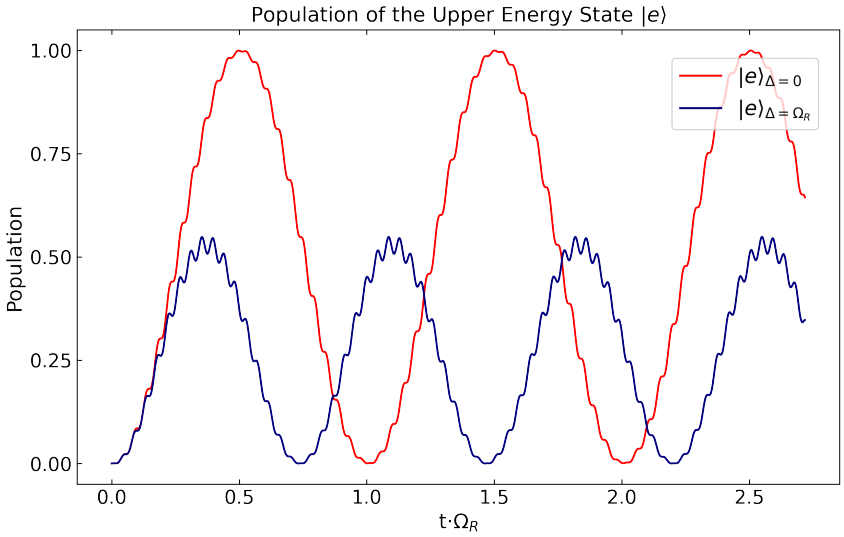

Figure 8: The influence of Rabi oscillation on the upper energy level population (computed with the Runge-Kutta Method): A comparison of the occupation progression with $\Delta = 0$ (marked in red) and $\Delta = \Omega_R$ (marked in blue).

The oscillations caused by the counter-rotating terms also have a significant influence here: the population curves are cut off earlier than in Figure 5.
In order to investigate the reason for these oscillations in more detail, one forms the Fourier transformation of the population curves from the upper energy state. This gives an insight into the frequencies that interact with the system and have an possible impact on these oscillations.

The next section deals with this process, whereby a comparison between the Rotating-Wave Approximation and the Runge-Kutta method is drawn, especially to better identify the frequency influence.

3.1.3 The comparison of RWA and RK4

First we compare the Fourier spectra of the oscillating population in the upper level at the detuning $\Delta = 0$. On the one hand calculated with the Rotating-Wave Approximation and on the other hand computed with the Runge-Kutta method:

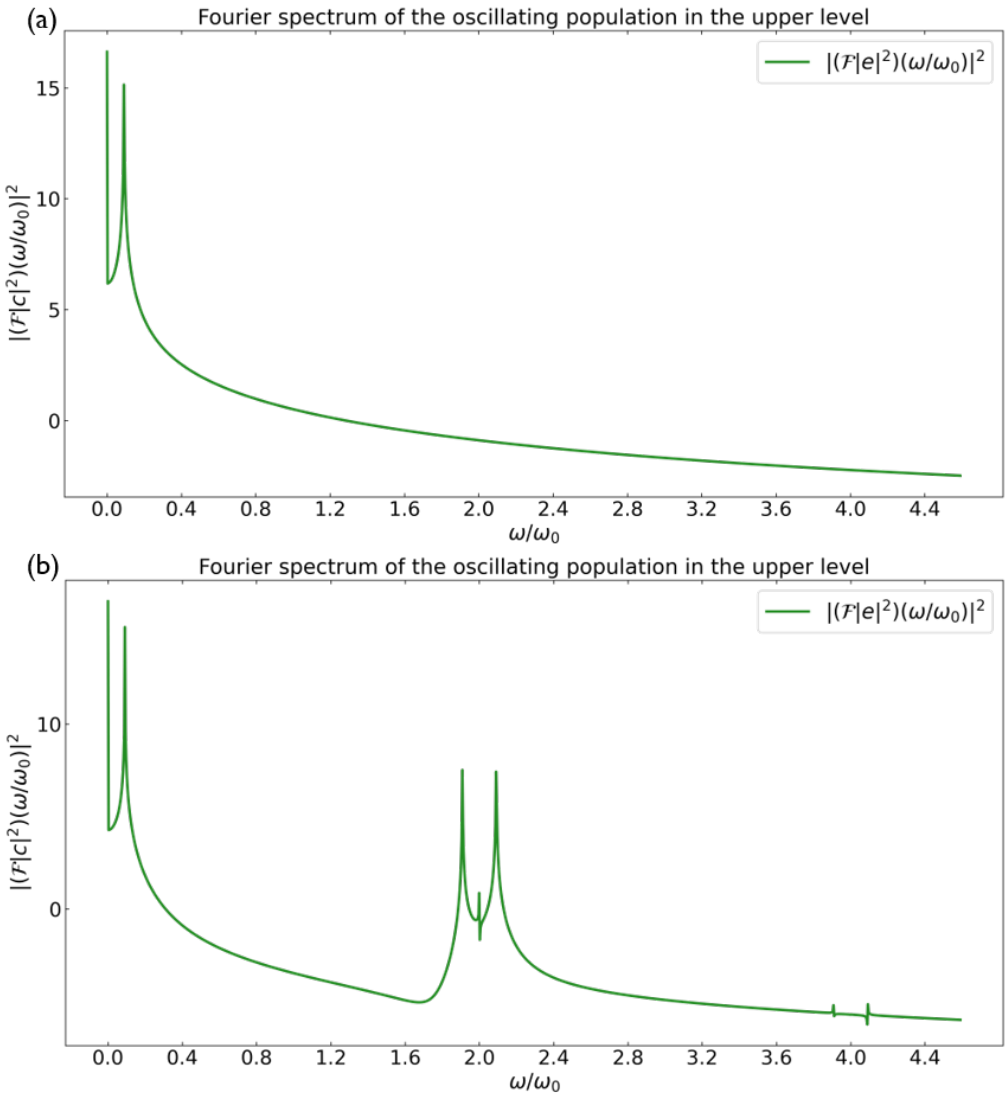

Figure 9: (a) Fourier spectrum of the oscillating population in the upper level determined with the Rotating-Wave Approximation. (b) Fourier spectrum of the oscillating population in the upper level determined by the Runge-Kutta method.

Here you can see a peak close to zero in both figures 9(a) and 9(b). This peak can be associated with the Rabi oscillation, which occurs in the Rotating-Wave Approximation and the Runge-Kutta method. However, in Figure 9(b) there are other peaks near $2\omega/\omega_0$ and $4\omega/\omega_0$.

To analyze this behavior further, first consider the Fourier spectrum, which was determined using the Rotating-Wave Approximation to focus on the first peak, and examine its intensity dependence.

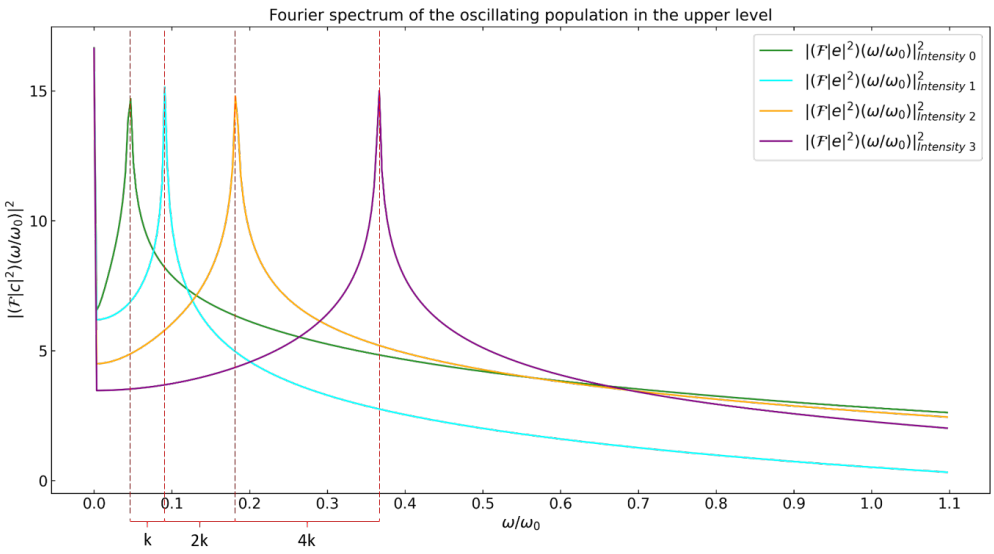

Figure 10: Fourier spectrum of the oscillating population in the upper level, determined with the Rotating-Wave Approximation, at different intensities. The initial intensity 'Intensity 0' ($0.5 \cdot E_0$) is doubled to 'Intensity 1' ($1 \cdot E_0$), quadrupled to 'Intensity 2' ($2 \cdot E_0$) and eightfold to 'Intensity 3' ($4 \cdot E_0$).

If the intensity is increased or decreased compared to the original intensity, the system oscillates faster or slower, correspondingly the Rabi oscillation is faster or slower. The upper energy level population oscillates at the Rabi frequency. If one changes the intensity of the incoming electric field $E(t)$, the Rabi frequency changes proportionally and thus the system oscillates slower or faster in proportion to the Rabi frequency. This can be seen in Figure 10: If the intensity is halved, doubled or quadrupled compared to the original intensity, a shift in the spectral lines to the left or to the right becomes visible. This means that changing the intensity causes a shift by the Rabi frequency: Doubling the intensity shifts the spectral line by $2 \cdot \Omega_R$ and quadrupling the intensity shifts the spectral line by $4 \cdot \Omega_R$ etc., therefore you can associate the first spectral line with the Rabi frequency.

Now examine the plot of Figure 9(b) and its spectral lines. For this purpose, the intensity dependency is also observed by plotting the Fourier spectrum of the oscillating population in the upper level, which was determined using the Runge-Kutta method, for different intensities.

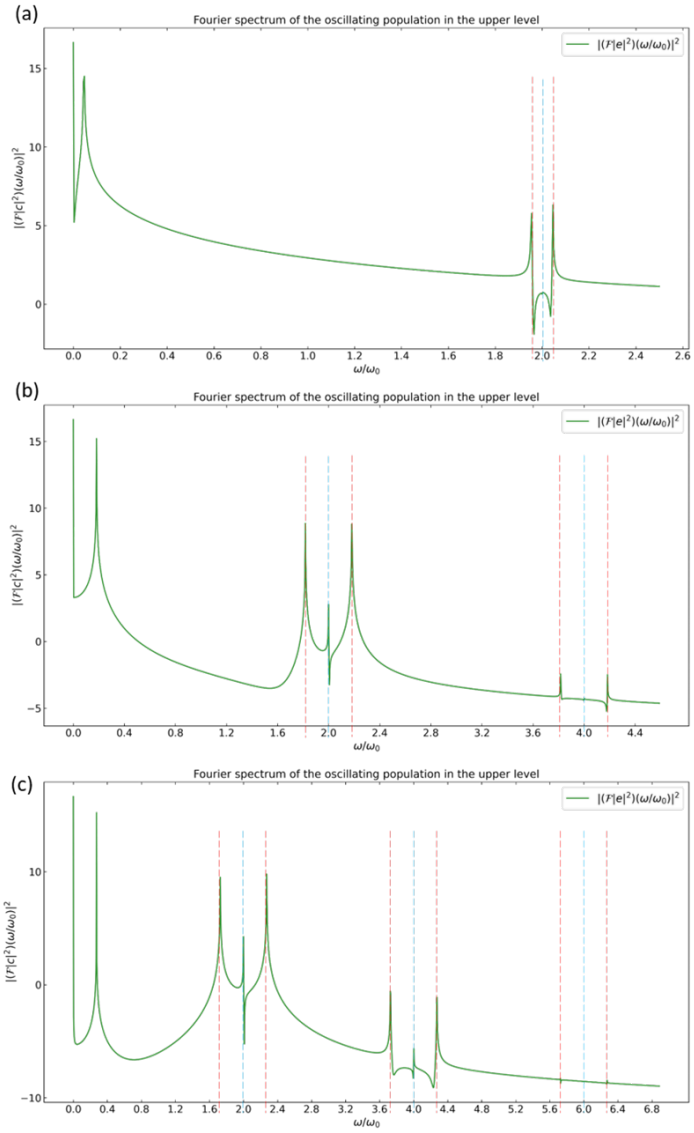

Figure 11: Fourier spectrum of the oscillating population in the upper level, determined with the Runge-Kutta Method, at different intensities. (a) shows the spectrum for the original intensity $0.5 \cdot E_0$, (b) four times the original intensity $2 \cdot E_0$ and (c) eight times the original intensity $4 \cdot E_0$.

Figure 11 shows not only a shift in the spectral lines, but also a splitting of the spectral lines. This is reminiscent of the Autler-Townes effect or AC Stark splitting. This effect describes the shifting and splitting of the spectral lines of atoms or molecules caused by the interaction with an external electric field. It must also apply that the excitation frequency (of the electric field) is close to the resonance frequency.

In Figure 11 above you can see a shift close to zero and a splitting and shift of the spectral lines at a distance of $2\omega/\omega_0$ from each other. A distance of $2\omega/\omega_0$ can be explained by the fact that the rapidly rotating terms oscillate with $2\omega_0$, because for the case $\Delta = 0$ is $\omega_{eg} = \omega_0$. Any spectral lines that only occur in the Runge-Kutta spectrum are thus assigned to an oscillation of the rapidly rotating terms. The other spectral lines at $4\omega/\omega_0$ and $6\omega/\omega_0$, which appear when the intensity is increased, can be associated with the 3-photon, 5-photon, etc. transition. For the 3-photon transition the rapidly rotating terms oscillate with $3\omega_{eg} + \omega_0 = 4\omega_0$ and the 5-photon transition the rapidly rotating terms oscillate with $5\omega_{eg} + \omega_0 = 6\omega_0$.

The intensity in Figure 11(b) and 11(c) has been quadrupled and eightfold, respectively, relative to Figure 11(a). It is noticeable that the splitting of the spectral lines expands outwards (red lines can be seen in the figure, which are getting further and further away from the blue lines). The shift also changes proportionally to the Rabi frequency, which is significally larger than ω_0 what explains why the outer spectral lines are larger. The spectral lines shift and thus split with the Rabi frequency Ω_R.

After applying the Rotating-Wave Approximation and the Runge-Kutta method to a two-level atomic system and comparing the two methods, one comes to the conclusion: The neglect of the rapidly rotating terms in the Rotating-Wave Approximation makes only an application in the near-resonance case, which is why in the further course of the thesis, the Runge-Kutta method is continued.

3.2 Pulsed Rabi oscillations in Two-Level Systems

In this chapter one deals with the interaction of an electric field $E(t)$ and a 2-level atomic system. However, it is no longer the case that the electric field $E(t)$ is continuous, but the incoming field is defined as an Pulse with pulse area A(t):

$$A(t) = \int_0^t dt' |D_{eg}| \cdot I(t')/\hbar \tag{35}$$

where $I(t')$ is the envelope of the pulse's electric field and $|D_{eg}|$ the system's electric dipole moment, the system undergoes coherent oscillations between its ground state $|g\rangle$ and the upper state $|e\rangle$.

Now consider the oscillation of the 2-level system, which interacts with a pulse of an electric field $E(t)$. The population probability is displayed with different pulse areas.

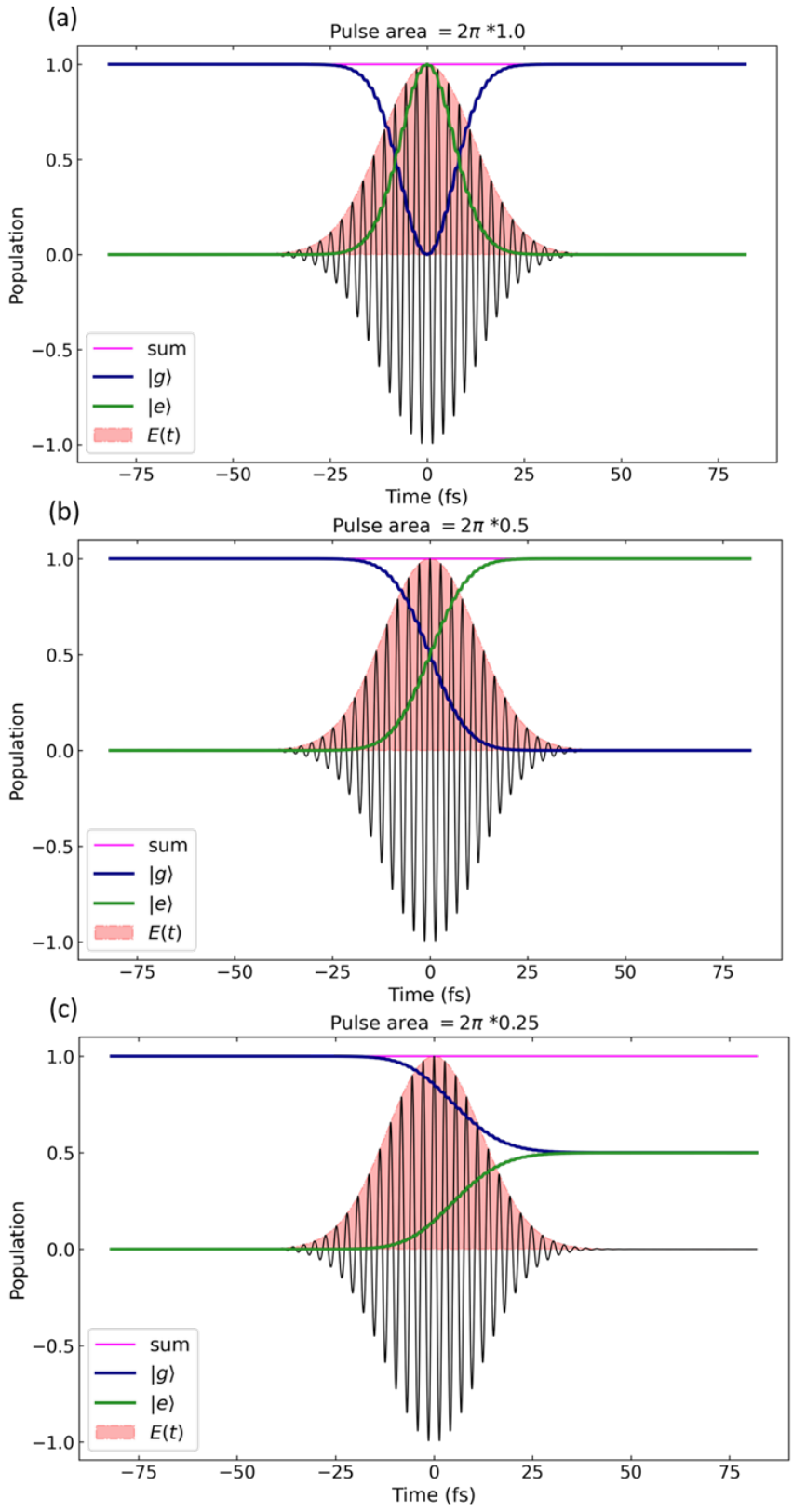

Figure 12: The Population of the ground state and the upper state. **(a)** The 2-Level system after an interaction with an pulse of Pulse Area 2π, **(b)** with an pulse of Pulse Area π and **(c)** with an pulse of Pulse Area $\pi/2$.

(a) shows the case for an interaction of a pulse, which has a pulse area of 2π, with the 2-level system. It can be seen that the population of the ground state first decreases due to the incoming pulse, so that $|g\rangle$ is no longer occupied, and then increases again until the ground state is completely populated. This means that the incoming pulse with a pulse area of 2π has caused a state change, namely:

$$|g\rangle \xrightarrow{2\pi} -|g\rangle \xrightarrow{2\pi} |g\rangle \tag{36}$$

.
The ground state $|g\rangle$ is thus transformed into the state -$|g\rangle$. The sign does not affect the population probability, as you can see the population probability is the same before and after the interaction with the pulse. However, a 2-level system is invariant to a 4π pulse [27,30].
Therefore, the ground state would return to the initial state after repeated interaction with a pulse having a pulse area of 2π, or when the system initially interacts with a pulse having a pulse area of 4π or a multiple thereof.
The following also applies to the upper state $|e\rangle$:

$$|e\rangle \xrightarrow{2\pi} -|e\rangle \xrightarrow{2\pi} |e\rangle \tag{37}$$

and for a superposition of the two states $|g\rangle$ and $|e\rangle$ one gets the result:

$$\alpha|g\rangle + \beta|e\rangle \xrightarrow{2\pi} -\alpha|g\rangle - \beta|e\rangle = -(\alpha|g\rangle + \beta|e\rangle). \tag{38}$$

(b) shows the interaction of a pulse, which has a pulse area of pi, with a 2-level system. Here it is easy to see that the population probability of the states $|g\rangle$ and $|e\rangle$ is swapped, giving the following state change:

$$|g\rangle \xrightarrow{\pi} i|e\rangle \tag{39}$$

$$|e\rangle \xrightarrow{\pi} i|g\rangle \tag{40}$$

The transitions between the two states ensure that the population probability of the ground state decreases until it is no longer populated, i.e. it has the initial population probability of $|e\rangle$. Likewise, the population probability of the upper state increases until it reaches the initial population of the ground state.

For the third case **(c)** consider an interaction of a pulse, which has a pulse area of $\pi/2$, with the 2-level system. The population probability decreases from the ground state and increases from the upper state, so that the two states are equally occupied after the interaction. This leads to a superposition state:

$$|g\rangle \xrightarrow{\pi/2} 1/\sqrt{2}(|g\rangle + i|e\rangle) \tag{41}$$

$$|e\rangle \xrightarrow{\pi/2} 1/\sqrt{2}(|g\rangle + i|e\rangle) \tag{42}$$

In this section the interaction of a 2-level system with a pulse was observed, whereby the pulse areas of the pulse were varied. As expected, after the interaction the system is in a different state depending on the pulse area.

3.3 Multiphoton Transitions

In this section consider the distribution of the upper energy level population depending on the number of photons interacting with the 2-level system. Accordingly, one considers which photon transitions are possible between the ground state and the upper energy state, or how probable different photon transitions are.

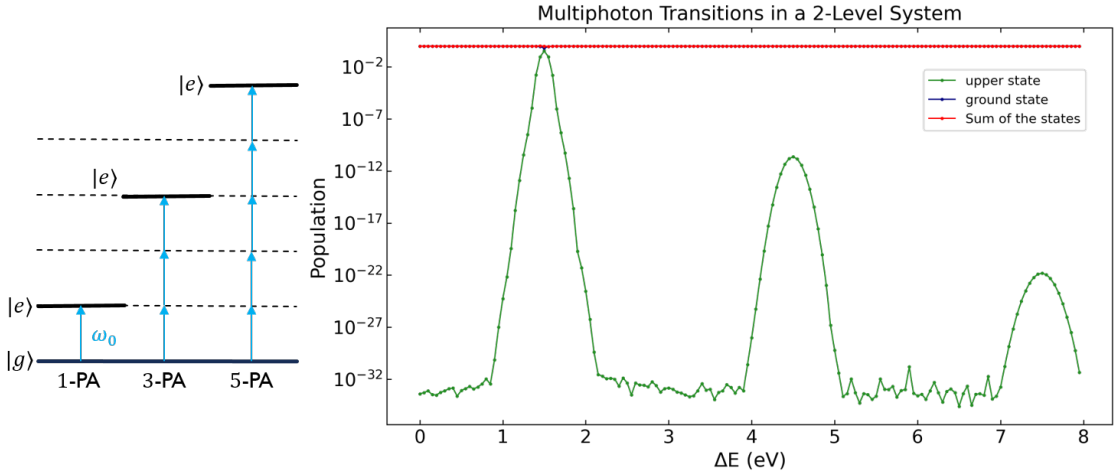

Figure 13: Population probability (log.) of the upper state of a two-level system as a function of the level spacing. In addition to the 1-photon absorption, the 3-photon absorption and the 5-photon absorption can also be seen. At about 10^{-30} is the limit to numerical noise.

In Figure 14, the upper energy level population is plotted as a function of the energy difference between the ground state and the upper energy state. It is an interaction with a photon source and a 2-level system, where the photon energy is as above $E_{ph} = 1.5eV$. Three population peaks can be seen at the same distance from each other, which decrease with increasing energy difference from the ground state to the upper state.

The peaks always occur at an odd multiple of 1.5 eV. At even multiples of 1.5 eV, the upper state is unpopulated. This means that only an odd number of photons can be absorbed and that as the number of photons increases, the probability of a transition decreases. An even number of photons cannot be absorbed or it is very unlikely.

The first maximum is seen at an energy level difference of 1.5 eV, which corresponds to a 1-photon transition. In addition, maxima at 4.5eV and 7.5eV are visible, which can be assigned to the 3-photon and 5-photon absorption.

3.3.1 Parity inversion symmetry of the Energy States

The parity inversion in three dimensions is described by:

$$P : \begin{pmatrix} x \\ y \\ z \end{pmatrix} \mapsto \begin{pmatrix} -x \\ -y \\ -z \end{pmatrix} \tag{43}$$

A parity inversion is the reversal of direction of a spatial coordinate, corresponding to a change of sign. It can also refer to reversing the sign of all three space coordinates at once. A distinction is made between a symmetrical $f(-\vec{r}) = f(\vec{r})$ and an anti-symmetrical $f(-\vec{r}) = -f(\vec{r})$ parity inversion.

Referring now to energy states, one defines a parity operator:

$$\Pi \left|x\right\rangle = \left|-x\right\rangle . \tag{44}$$

Considering the effect of a parity operator on a quantum state, in this case an energy state:

$$\Pi \left|\psi\right\rangle = \left|\psi'\right\rangle \quad \text{and} \quad \psi'(x) = \psi(-x). \tag{45}$$

If one examines the eigenstates of the parity operator, one comes to the conclusion that there are two, namely +1 and -1:

$$\Pi \left|\pi\right\rangle = \pi \left|\pi\right\rangle \quad \text{and} \quad \pi = \pm 1. \tag{46}$$

A distinction is made between the two eigenstates, an even state $\pi = +1$ and an odd state $\pi = -1$. Based on the effect of the parity operator on a state, the energy states are divided into even (+) and odd (-) states.

In order to understand the relationship between the parity operator and the Hamiltonian, one determines the commutator

$$[\Pi, \mathcal{H}] = 0. \tag{47}$$

Therefore simultaneous eigenstates of Energy and Parity must exist.
Finally, one comes to the conclusion that the energy states alternately have a symmetric and an antisymmetric parity inversion

$$\Pi \left|n\right\rangle = (-1)^n \left|n\right\rangle . \tag{48}$$

Accordingly, in a 2-level system there are two energy levels with different parity inversion symmetry. However, a 2-photon transition is only possible between 2 energy levels with the same parity inversion symmetry.

It depends on how one defines the parity of the atomic energy levels. This thesis deals with a 2-level atomic system whose energy states have even and odd parity. Accordingly, only an odd number of photons can be absorbed.

3.4 2-Level System with Decay

In this section consider a 2-level atomic system with decay. More specifically, the decay of the excited state population. A 2-level system interacts with a pulse of an electric field, which has a pulse range of 4π. For this we define a factor γ which ensures that the population of the excited state decays. This is taken into account in the equation of motion c_e, so that one gets:

$$\dot{c}_e(t) = i\Omega R c_g \frac{exp(i\Delta t - i\varphi) + exp(i|\omega_{eg} + \omega_0|t + i\varphi)}{2} - \gamma \cdot c_e. \tag{49}$$

We consider two cases for the decay of the excited state population: firstly, the population decreases and ionization occurs, i.e. the total population decreases over time, and secondly, the decay of the excited state to the ground state is added to it, whereby the population of the excited state is transferred to the ground state. In the second case, the total population remains constant at 1. One then gets for the equation of motion of c_g:

$$\dot{c}_g(t) = i\Omega R c_e \frac{exp(i\Delta t + i\varphi) + exp(i|\omega_{eg} + \omega_0|t - i\varphi)}{2} + \alpha \cdot \frac{|c_e|^2}{c_g^*}. \tag{50}$$

For the first case $\alpha = 1$ and for the second case $\alpha = 0$. The two equations of motion are solved using the Runge-Kutte method as given in section 3.1.2.

First, the population probability of the 2-level system with $\gamma = 0$ is shown:

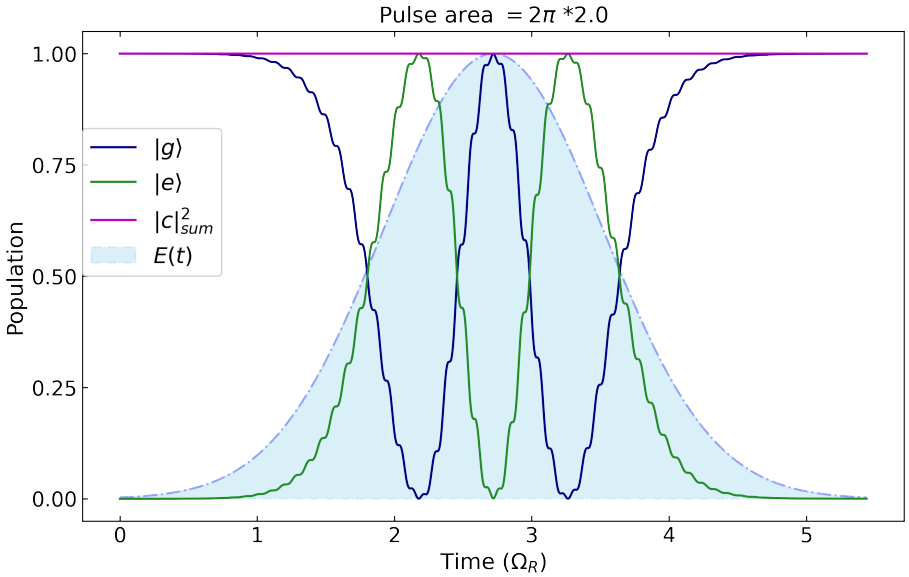

Figure 14: The Population of the ground state and the upper state, after an interaction with an pulse of Pulse Area 4π. In this case $\gamma = 0$ and the total population remains 1.

As expected, the population is periodic, with the system being in the ground state at $t = 0$ and returning to the initial state after the interaction with the electric field. The total population, in that case, remains constant 1 since there is no decay of the excited state population.

Now consider the case $\gamma = 4.17 \cdot 10^{-14}$ s:

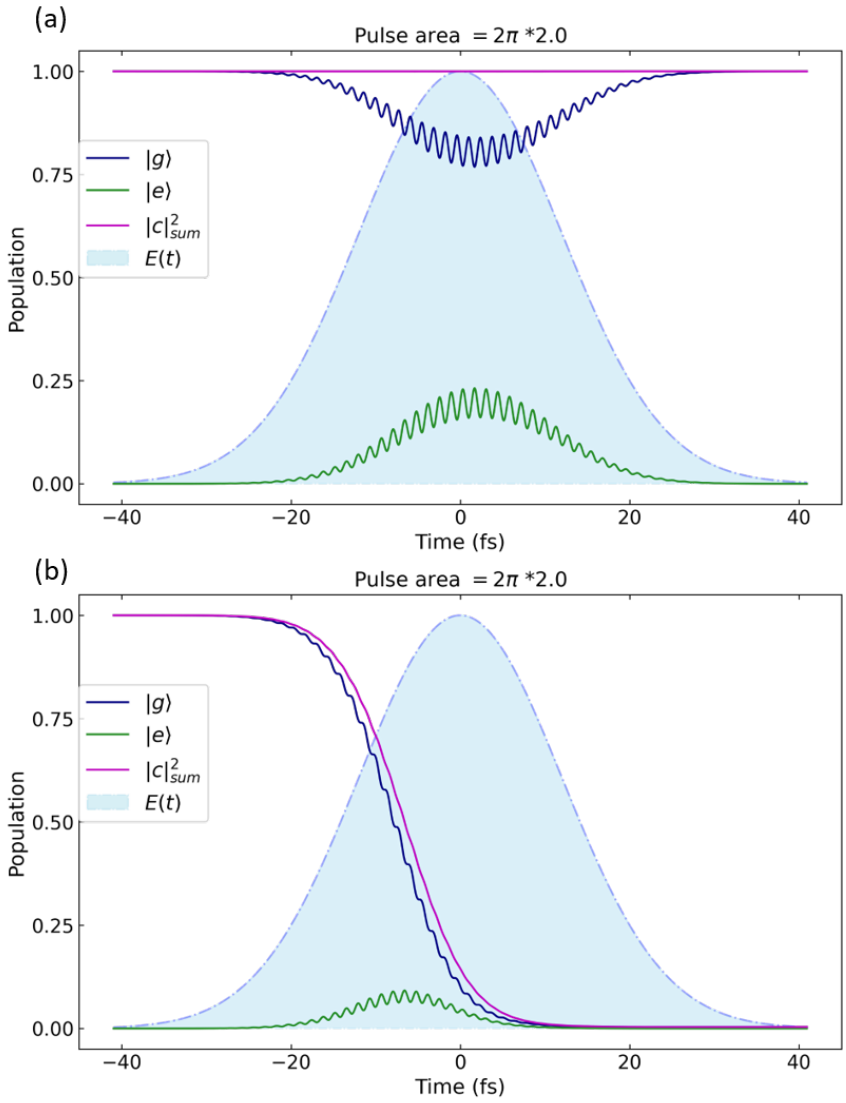

Figure 15: The Population of the ground state and the upper state, after an interaction with an pulse of Pulse Area 4π. For (a) the decay of the excited state is added to the ground state and for (b) the Population of the excited state decreases because of ionisation.

In Fig. 15(a) one can now see that the decay from the excited state to the ground state is added and the total population remains constant at 1. The upper energy level population increases only slightly and then eventually decays, returning the system to the ground state. In Fig. 15(b), the total population decreases with time because the decay of the upper energy level population is not carried over to the ground state.

In the appendix (A.5) there are further representations for lower values of γ.

In this chapter one comes to the conclusion: After testing two different methods (RWA and RKM) for the calculation of the equations of motion for the groundstate and the excited state, the Runge-Kutta method proves to be better. The Rotating-Wave Approximation is only applicable to near-resonance cases, since the fast-rotating terms can no longer be neglected for a detunig $\Delta >> 0$. In the further course of the thesis, the Runge-Kutta method was continued. Then the 2-Level system is tested with a pulse with different pulse areas. One came to the result: For a 2π pulse the system is again in the initial state after the interaction, with a π pulse the system is in the excited state and at a $\pi/2$ pulse, the system is in a superposition of the ground state and the excited state. Furthermore, multiphoton transitions were examined. An even number of photons is not absorbed (because of inversion symmetry), or the probability of this is very low. The probability of a transition also decreases, the larger the number of photons is: This means that a 1-photon absorption is more likely than a 3-photon absorption or a 5-photon absorption, etc. At the end of this chapter, a 2-Level System with decay was considered. Here we have distinguished between two cases: the decay of the excited state is added to the ground state or the population of the excited state decays but is not added to the ground state, instead ionization occurs. In the first case the total population remains constant 1 and in the second case the total population decreases over time.

4 The 5-Level System

In this chapter we will focus on the Population probability per time of each energy state in an 5-Level System. On the one hand for a constant energy difference between the states and on the other hand for an densification of the upper states. In this case, the term 5-level system stands for 5 upper energy levels, with the ground level being referred to as the 0th level. The aim is to approximate these "higher energy states" into continuum states, by adding more number of closely spaced energy levels near to the resonance states.

For the 5-Level System we can define the wave function of the unperturbed system according to (24):

$$|\psi(t)\rangle = \sum_{k=0}^{5} c_k(t)\,|k\rangle\,, \tag{51}$$

and therefore we can now describe the Hamiltonian with the coupling between the 6 states $D_{kl} = \langle k|\,\mathcal{H}_{int}(t)\,|l\rangle$ on the off-diagonal, according to (25):

$$\mathcal{H} = \begin{pmatrix} E_0 & D_{01} & D_{02} & D_{03} & D_{04} & D_{05} \\ D_{10} & E_1 & D_{12} & D_{13} & D_{14} & D_{15} \\ D_{20} & D_{21} & E_2 & D_{23} & D_{24} & D_{25} \\ D_{30} & D_{31} & D_{32} & E_3 & D_{34} & D_{35} \\ D_{40} & D_{41} & D_{42} & D_{43} & E_4 & D_{45} \\ D_{50} & D_{51} & D_{52} & D_{53} & D_{54} & E_5 \end{pmatrix}, \qquad |\psi\rangle = \begin{pmatrix} c_0(t) \\ c_1(t) \\ c_2(t) \\ c_3(t) \\ c_4(t) \\ c_5(t) \end{pmatrix}. \tag{52}$$

With the dipole approximation we can evaluate the matrix elements D_{kl} and get a formal solution for the Schrödinger equation as stated by (26) and (27).

In this chapter, a distinction is made between a continuous electric field E(t) that interacts with a 5-level system and the interaction with a pulse with a pulse area of 2π, as for the 2-Level System.

In both illustrations we will use the Runge-Kutta Method (RK4) for solving the equations of motion c_k (for $k, l \in \{0, ...5\}$) as explained for the Two-Level System:

$$\dot{c}_k(t) = 1/i\hbar \sum_l c_l D_{kl} E(t) \exp\left(-i(\omega_l - \omega_k)t\right) \tag{53}$$

For this chapter assume a dipole coupling element of $D_{kl} = 0.5 \cdot 10^{-28}\ Cm$ an intensity of the continuous electric field of $E_0 = 22 \cdot 10^8\ V/m$ and the initial conditions $c_g(0) = 1$ and $c_{e_i}(0) = 0$ for $i \in \{1, ...5\}$ and all couplings between the states are allowed, except for D_{kk}.

4.1 Atom-Light Interaction with a continuous field $E(t)$

An continuous electric field $E(t)$, which oscillates with an frequency ω interacts with a 5-Level System. Depending on the energy difference between the various energy states and the initial conditions, the individual states are either excited or decay over time. This changes the population of the states and you get a population distribution of the individual states.

4.1.1 Constant energy difference between the energy states

In this section we look at a 5-Level System, in which the energy difference to the next energy state is constantly the same, namely a multiple of the energy of the electric field $E_{ph} = \omega\hbar/e = 1.5\ eV$.

First we consider a the frequency difference of ω between each state, then a frequency difference of $\omega/2$ and finally of $\omega/4$.

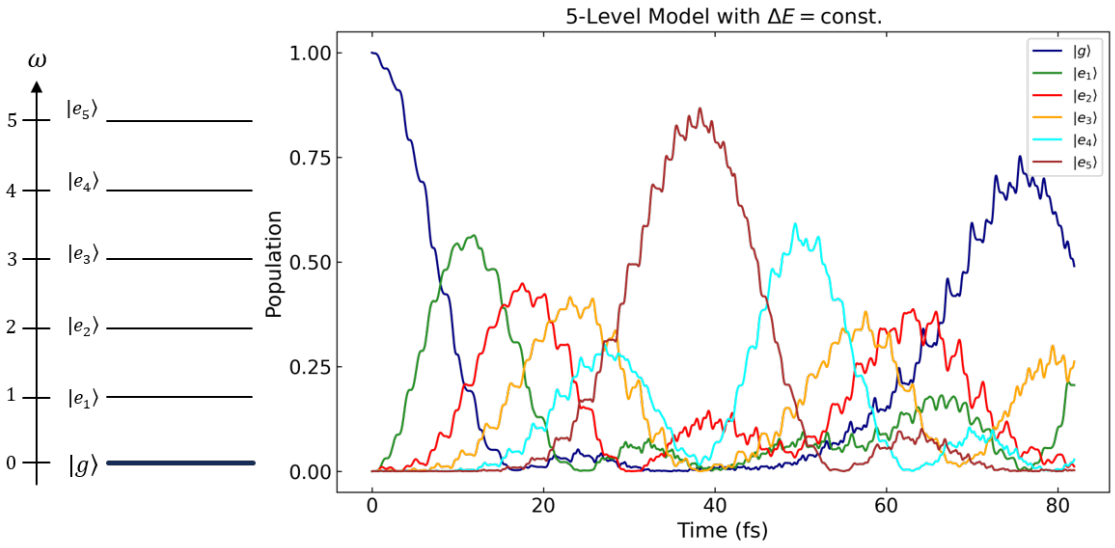

Figure 16: The population of energy states in a 5-level system interacting with a continuous electric field $E(t)$, which is oscillating with the frequency ω. The frequency difference between the levels is constant ω.

According to the initial condition $c_g(t = 0) = 1$ one can see that the ground state is at the beginning, before the electric field interacts with the system, fully populated, while the upper states are at the beginning $t = 0$ not populated $c_{e_i}(t = 0) = 0$.

At $t > 0$ the population of the ground state decreases, while the first upper state $|e_1\rangle$ gains population until it is around 55% populated. After its population peak, $|e_1\rangle$ decreases in population as fast as it gained population.
The following states $|e_2\rangle$, $|e_3\rangle$ and $|e_4\rangle$ increase in population slower than $|e_1\rangle$. In order from the lowest energy state $|e_2\rangle$ to the highest energy state $|e_4\rangle$, the states increase more slowly and have a lower population peak the higher the energy state is.
The reason for this distribution is that the frequency difference of the energy states is exactly the frequency of the electric field ω and that we start with a fully populated ground state. When the field E(t) interacts with the system the first upper state is most likely to be excited and it is not very likely that at the very beginning the second upper state is excited. The probability of occupying a state at the beginning of the interaction decreases as "higher" the energy state is.

While the first upper state is populated, the field E(t) continues to interact with the system, so the probability of occupying the second energy state increases. As $|e_2\rangle$ gains more Population and the 5-Level System interacts with a continuous field, the probability of occupying the third energy state increases and so on.

Focusing again on the ground state, one can see that after each of the upper states $|e_1\rangle$ to $|e_4\rangle$ started to get populated, the population of $|g\rangle$ is close to zero. The sum of the Population of all states in the system has to be $\sum_{k=0}^{5} |c_k(t)|^2 = 1$ and when the ground state is not populated anymore, it is because the upper states together are fully populated.

While the population of $|e_4\rangle$ is increasing, the "highest" upper state $|e_5\rangle$ starts to get populated. At this time the population of $|g\rangle$ and $|e_1\rangle$ is very low. In addition to that $|e_2\rangle$, $|e_3\rangle$ and $|e_4\rangle$ decrease in population, so that at the peak of $|e_5\rangle$ the other states are barely populated, which causes $|e_5\rangle$ to be over 70% populated at its peak.
In the time frame in which $|e_5\rangle$ is occupied, you can also see that $|e_1\rangle$ and $|e_2\rangle$ have a second small peak right after the the ground state has a very small peak. One can therefore assume that the levels $|e_1\rangle$ and $|e_2\rangle$ are in an excited state due to absorption from the ground state on the one hand and spontaneous emission from the higher states $|e_3\rangle$ and $|e_4\rangle$ on the other.

After $|e_5\rangle$ reaches its peak, the population by emission decreases, making $|e_4\rangle$ more populated and also decreasing in population by spontaneous emission after its peak. During this process, the ground state continues to increase in population.

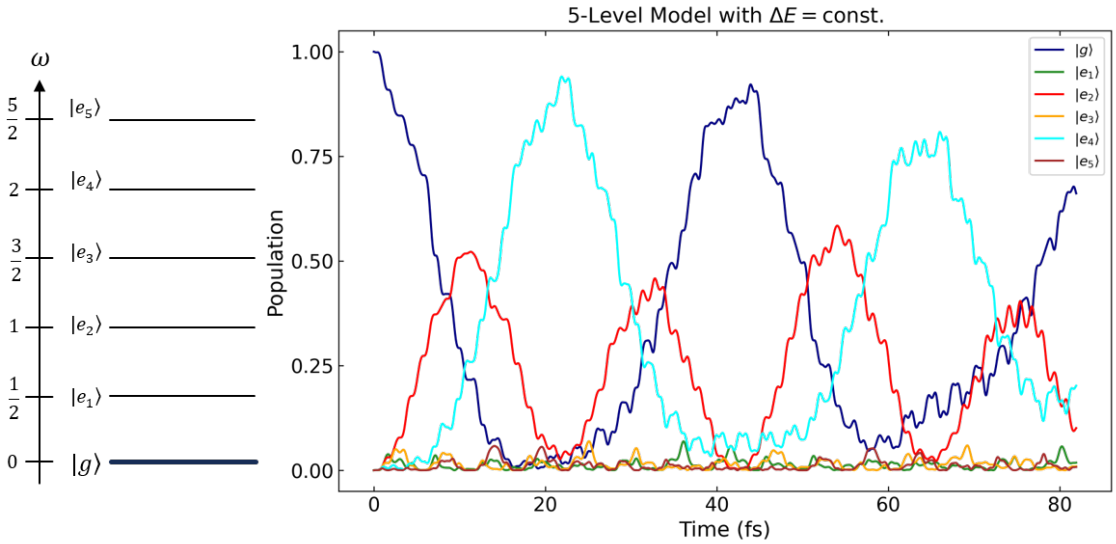

Figure 17: The population of energy states in a 5-level system interacting with a continuous electric field $E(t)$, which is oscillating with the frequency ω. The frequency difference between the levels is constant $\omega/2$.

This shows a 5-level system in which the respective states have a frequency difference of $\omega/2$, i.e. half the frequency of the incoming field $E(t)$. This means that the states $|e_4\rangle$ and $|e_4\rangle$ are more likely to be occupied, since transitions are only allowed between discrete energy levels, namely for $\Delta\omega_{xy} = a \cdot \omega$ with $a \in \mathbb{N}$ and $\Delta\omega_{xy}$ being the transition frequency between two different states.

The field $E(t)$ also interacts with the field when the ground state is completely occupied and the remaining states are unpopulated.
What is immediately noticeable is that the states $|e_1\rangle$, $|e_3\rangle$ and $|e_5\rangle$ are hardly occupied throughout. However, one recognizes that these states oscillate close to 0, which is due to the fact that the frequency ω is small and the frequency difference between the states is therefore also very small. If you increase the frequency, the oscillation decreases and the states $|e_1\rangle$, $|e_3\rangle$ and $|e_5\rangle$ have no population. As already mentioned above, only the transition between the ground state and the two states $|e_2\rangle$ and $|e_4\rangle$ is allowed.

At the beginning one sees the transition from the ground state to the second upper state. Due to the continuous interaction with the electric field $E(t)$, further transitions from the already occupied state $|e_2\rangle$ to $|e_4\rangle$ as well as $|g\rangle$ to $|e_4\rangle$ take place. This can be seen by the fact that the population of the ground state decreases and the population of the second upper state increases first, which then leads to the population of the highest possible state $|e_4\rangle$ increasing even more. Since $|e_4\rangle$ is the highest possible state that can be populated and the transitions to a higher level by absorption caused by the electric field outstrip the transitions to a lower level by emission, its population increases up to the remaining states have reached their minimum. $|e_4\rangle$ even peaks higher than in Figure 17, caused by there being fewer states to populate.

Because of stimulated emission caused by the field and spontaneous emission, the population of $|e_4\rangle$ decreases and transitions directly to the ground state take place, as well as transitions with a diversion via $|e_2\rangle$ to the ground state. Now the population of $|g\rangle$ increases significantly until it is completely occupied. This whole cycle eventually starts all over again.

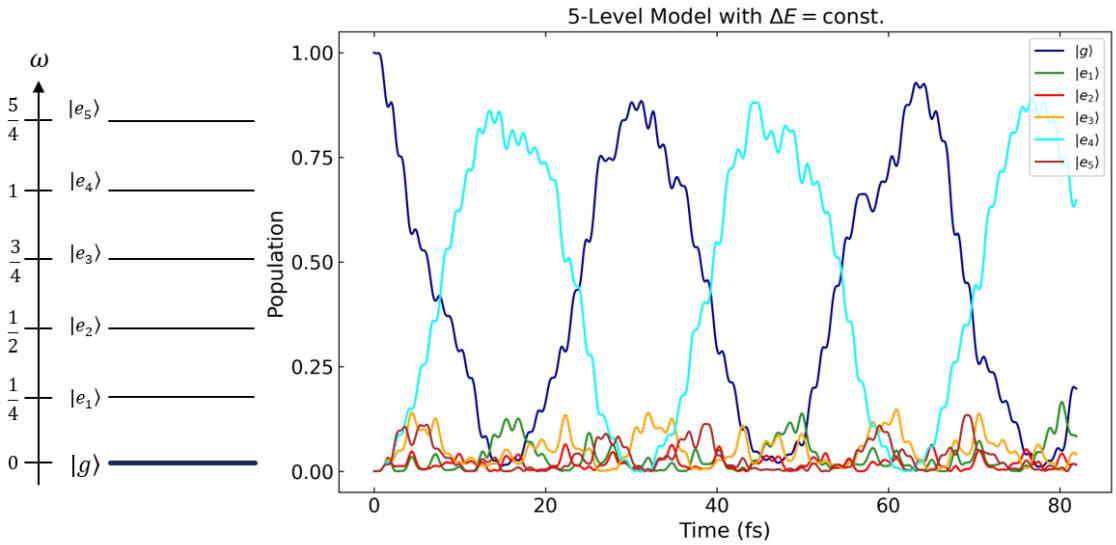

Figure 18: The population of energy states in a 5-level system interacting with a continuous electric field $E(t)$, which is oscillating with the frequency ω. The frequency difference between the levels is constant $\omega/4$.

Figure 19 shows a very similar distribution to Figure 18, with the difference that the energy states have an even smaller frequency difference, namely $\omega/4$ each. In that case $|e_4\rangle$ is the only state besides the ground state that can be occupied. As a result, only these two states oscillate in the system. You can also see that the oscillation of the states $|e_1\rangle$, $|e_2\rangle$, $|e_3\rangle$ and $|e_5\rangle$ is even more significant near 0 because the frequency difference is even smaller than in Figure 18.

4.1.2 Variation of the energy state distance

In this section we consider 5-level systems, which also interact with an continuous electric field $E(t)$, but with the difference that the energy states do not have the same frequency difference to each other, but we dense the upper states to the resonant state and then vary the frequency difference $\Delta\omega_{|e\rangle}$ between the upper states, keeping the frequency difference from the ground state to the resonant state constant.

Here we start with a relatively large value for $\Delta\omega_{|e\rangle}$, namely 0.1ω and then decrease the frequency by a factor of 10.

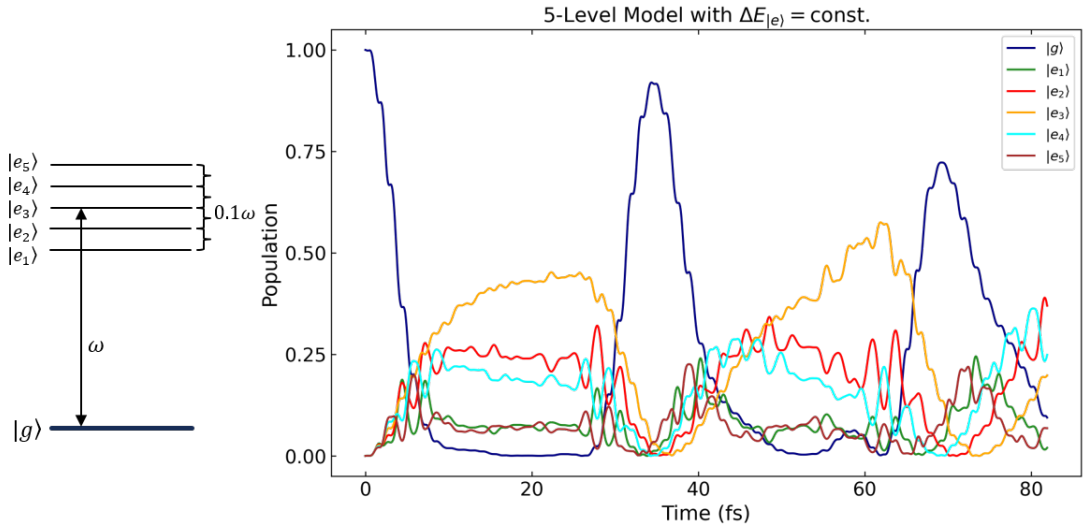

Figure 19: The population of energy states in a 5-level system interacting with a continuous electric field $E(t)$, which is oscillating with the frequency ω. The frequency difference between the upper levels is constant 0.1ω, while the ground state and the resonant state $|e_3\rangle$ differ by ω.

This is a 5-level system with a frequency difference of 0.1ω between the upper energy states. The frequency difference between the ground state and the resonant state $|e_3\rangle$ is ω. Because of the relatively large value of $\Delta\omega_{|e\rangle}$ there is a significant difference in the population of the upper energy states. The resonant state $|e_3\rangle$ dominates for all discernible population peaks. This is followed by the closest states $|e_2\rangle$ and $|e_4\rangle$, with the lower state being occupied a little more. As expected, the occupation of the energy levels, which have the greatest difference to the resonance frequency, is the lowest.

If you now dense the upper energy levels a little more, more precisely by a factor of 10, you have a frequency difference $\Delta\omega_{|e\rangle}$ of 0.01ω.

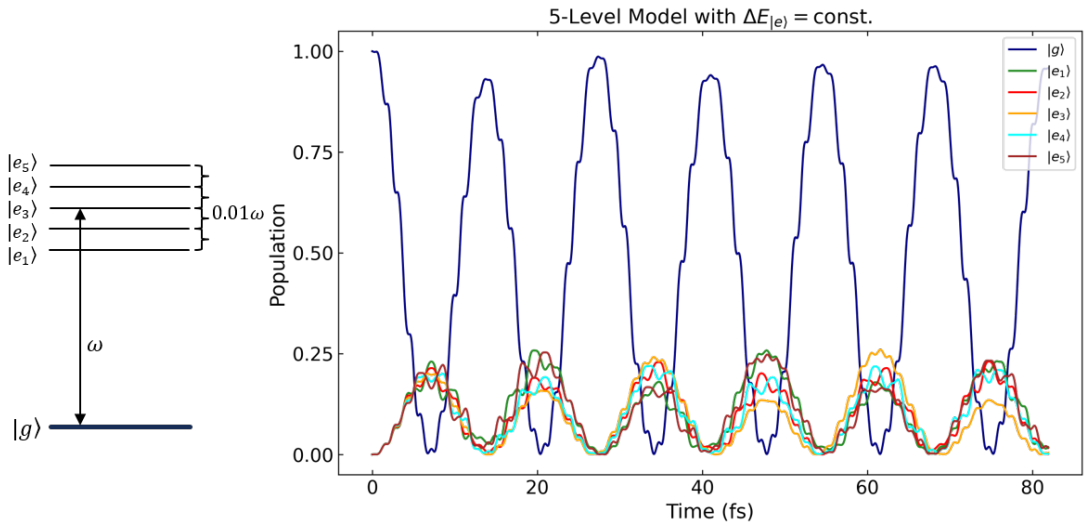

Figure 20: The population of energy states in a 5-level system interacting with a continuous electric field $E(t)$, which is oscillating with the frequency ω. The frequency difference between the upper levels is constant 0.01ω, while the ground state and the resonant state $|e_3\rangle$ differ by ω.

Here a different picture emerges as in Figure 20: As initially unexpected, the population of the resonant energy state $|e_3\rangle$ is not the most occupied. However, the energy levels in this case are very close, so that they hardly differ from the resonant energy level and the occupation of the levels seems arbitrary. The interaction with the 6-level system is similar to a 2-level system, with a wide frequency range of the upper energy level.

In the following figure, the frequency difference $\Delta\omega_{|e\rangle}$ is reduced even further, again by a factor of 10. It is therefore a distance of 0.001ω between the energy levels:

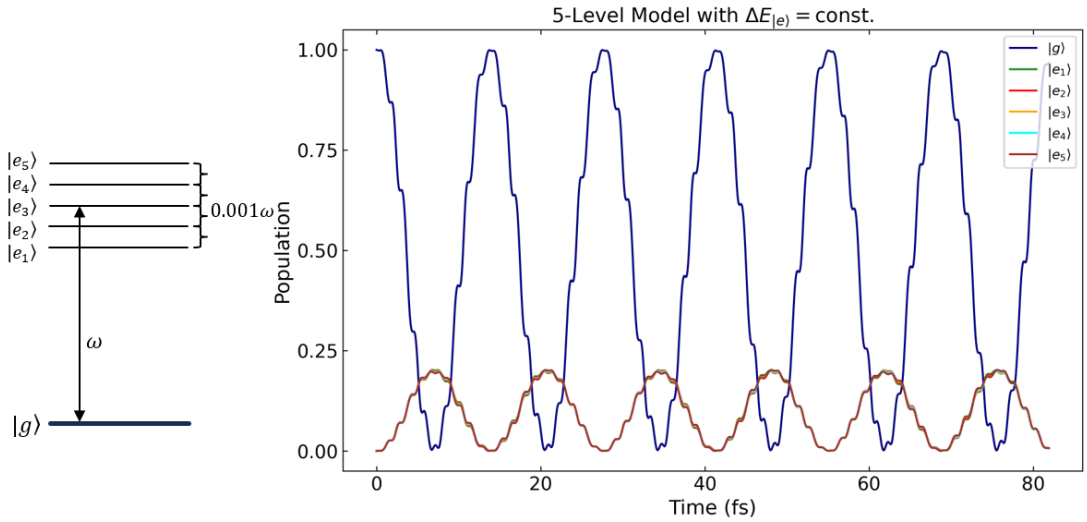

Figure 21: The population of energy states in a 6-level system interacting with a continuous electric field $E(t)$, which is oscillating with the frequency ω. The frequency difference between the upper levels is constant 0.001ω, while the ground state and the resonant state $|e_3\rangle$ differ by ω.

In Figure 22, the densification of the excited energy states becomes even more evident: the individual energy levels are so close to the resonant energy level that their populations oscillate with an almost indistinguishable frequency.

4.2 Atom-Light Interaction with a single pulse

In this chapter, as noted above, the 5-level system no longer interacts with a continuous electric field $E(t)$, but with a pulse of an electric field that has a pulse area of 2π.
A distinction is also made in the system between a constant distance between the energy levels and a densification of the upper energy levels.

4.2.1 Constant distance between the energy states

First consider the population of a 5-level system, in which the energy levels have a constant distance of ω to each other, so the excitation frequency and resonance frequency are the same $\omega_{eg} = \omega$.

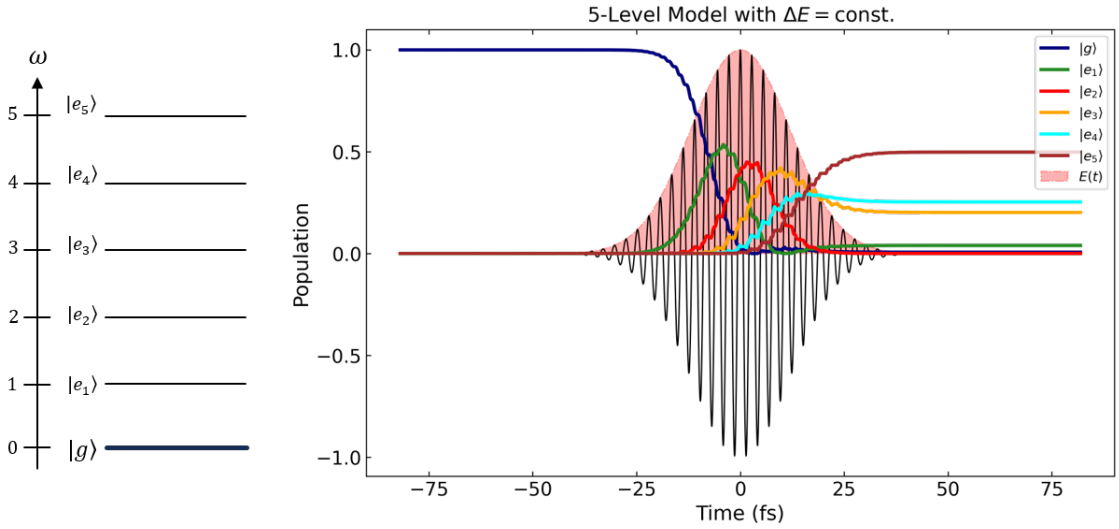

Figure 22: The population of energy states of a 5-level system interacting with a pulse that has a pulse area of 2π. The frequency difference between the levels is constant ω.

Unlike the 2-level system, the 5-level system is not in its initial state after interacting with the electric field $E(t)$. Because after the interaction, the population of the ground level is close to zero and the highest energy level $|e_5\rangle$ is the most populated. The final state of the system is thus a superposition of all energy states.

4.2.2 Variation of the energy state distance

Now consider a 5-level system with densed excited energy states, as in section (4.1.2) but with the difference that the system interacts with a pulse, which has a pulse area of 2π.

One starts again with a frequency difference of 0.1ω between the upper energy levels and a distance of ω to the resonant energy level and the ground level.

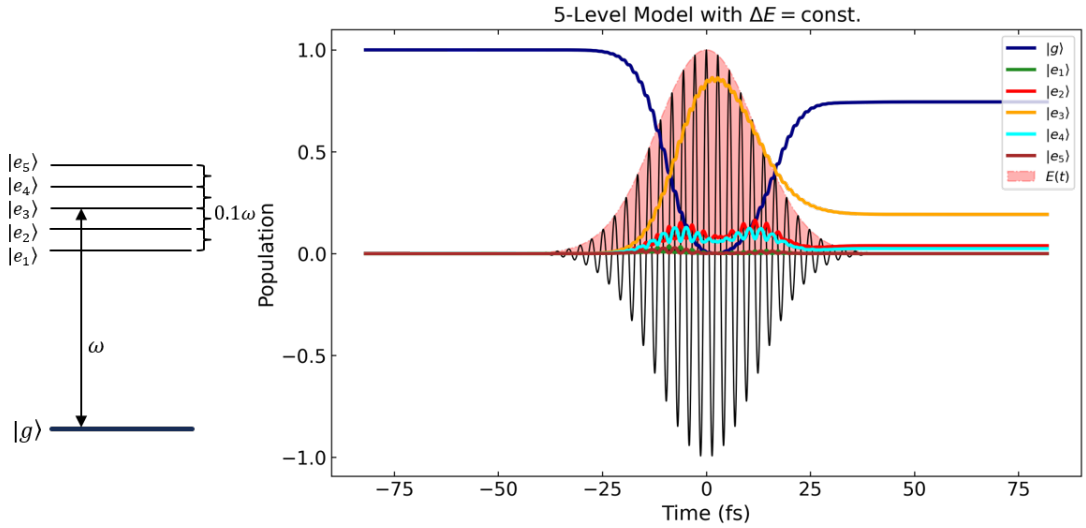

Figure 23: The population of energy states of a 5-level system interacting with a pulse that has a pulse area of 2π. The frequency difference between the upper levels is constant 0.1ω, while the ground state and the resonant state $|e_3\rangle$ differ by ω.

Here you can see very clearly that the transitions from the ground state to the resonant energy state $|e_3\rangle$ predominate and that the other energy states are hardly occupied. As expected, the probability of an energy level being populated is lower, the more its frequency distance to the ground level differs from the resonant frequency.

In the next two figures below, the frequency spacing of the upper energy levels is again reduced by a factor of 10. Accordingly, one gets a frequency spacing of 0.01ω and 0.001ω between the upper energy levels.

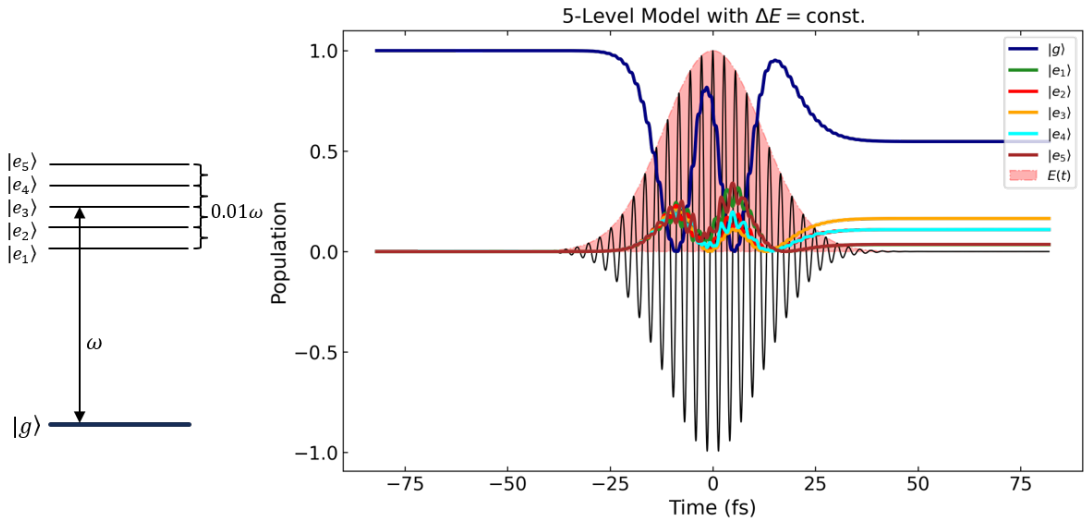

Figure 24: The population of energy states of a 6-level system interacting with a pulse that has a pulse area of 2π. The frequency difference between the upper levels is constant 0.01ω, while the ground state and the resonant state $|e_3\rangle$ differ by ω.

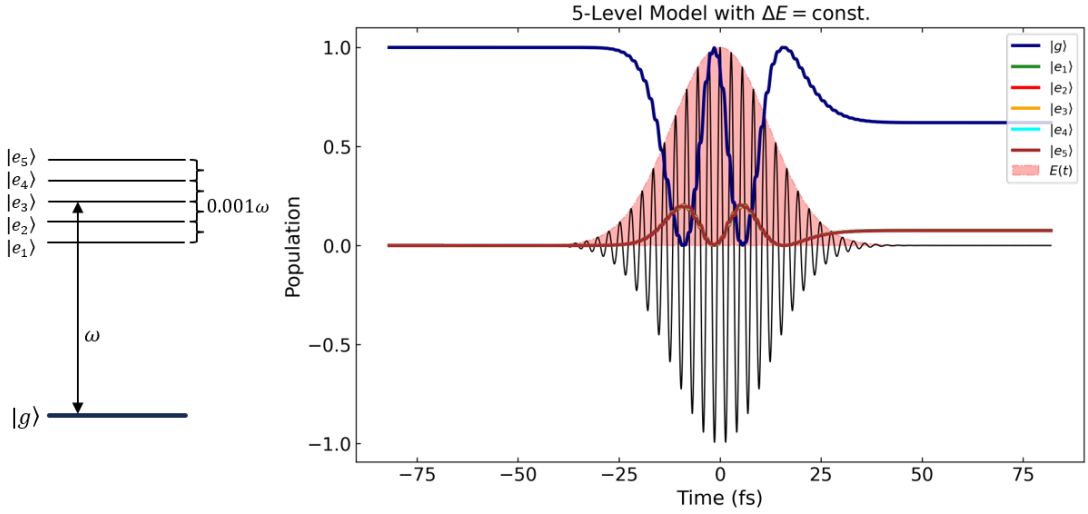

Figure 25: The population of energy states of a 6-level system interacting with a pulse that has a pulse area of 2π. The frequency difference between the upper levels is constant 0.001ω, while the ground state and the resonant state $|e_3\rangle$ differ by ω.

It becomes clear that the closer the upper energy levels are to each other, or the more one dense the upper energy levels, the more likely it is that each of the upper energy levels will be populated, since the distinction to the resonant energy level e_3 decreases. A comparison to the 2-level system (3.1) can be made, where it could be seen that with a very small detuning Δ, the probability of populating the upper energy level is greater. With a frequency difference of $0.001\omega_0$, the upper energy levels are so close to the resonant energy level that the populations appear almost identical and, as in Figure 22, the representation resembles a 2-level system.

5 RABITT

This chapter deals with the RABBITT pump-probe interferometry technique. In this technique, an atom (or gas) is ionized using an ultraviolet (XUV) attosecondpulse train (APT) and a time-delayed infrared IR pulse. If you look at the kinetic energy spectrum of the photoelectrons, caused exclusively by the XUV pulse, you can see discrete peaks, which are assigned to the harmonic peaks ("harmonics"). The IR pulse also causes sidebands to appear between the discrete harmonic peaks. In this chapter we limit ourselves to only one sideband between two discrete harmonic peaks. However, there are also RABBITT techniques with multiple sidebands between the harmonic peaks.

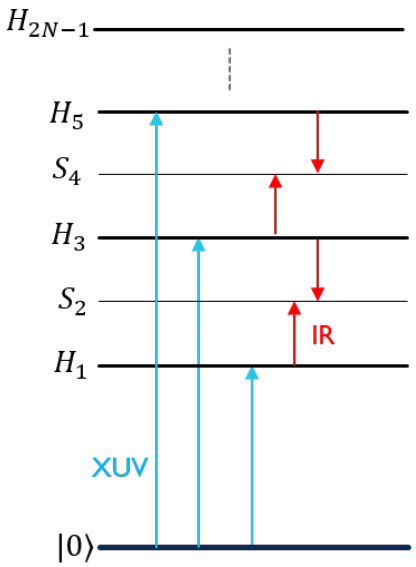

Figure 26: Energy-Level scheme in 1-SB RABBITT: The XUV APT (blue arrow) causes Photoionisation and the IR pulse (red arrow) causes the developement of the sidebands.

Furthermore, we now want to consider the RABBITT technique with one sideband between two harmonics: On the one hand for no chirped XUV pulse and on the other hand with an chirped XUV pulse.

5.1 RABBITT with no chirped XUV pulse

First consider the normalized energy spectrum as a function of the frequency, and the normalized field amplitude versus time. We chose a pump pulse containing nine odd harmonics (3,5,7,9,...,19) and get accordingly eight even sidebands (4,6,8,...,18).

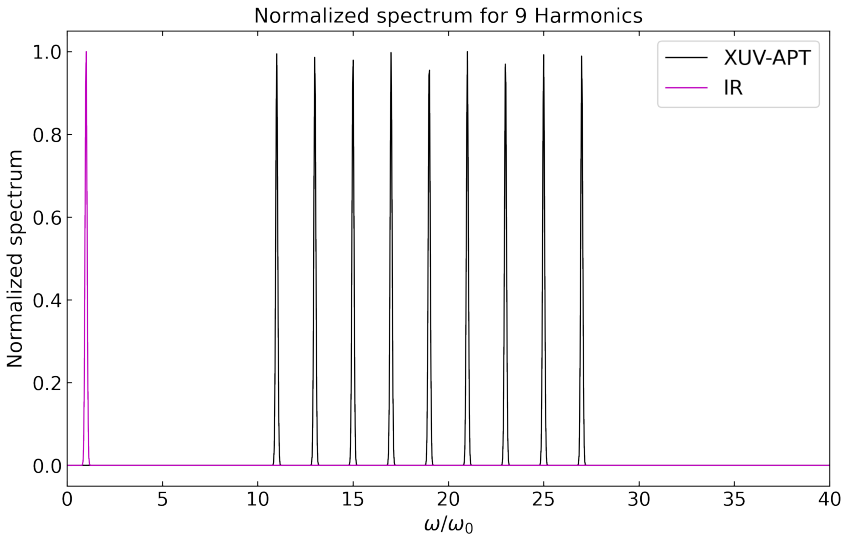

Figure 27: The normalized spectrum as a function of freequency. The 9 Harmonics (black peaks) are centered around $19\omega/\omega_0$ and are $2\omega/\omega_0$ apart from each other.

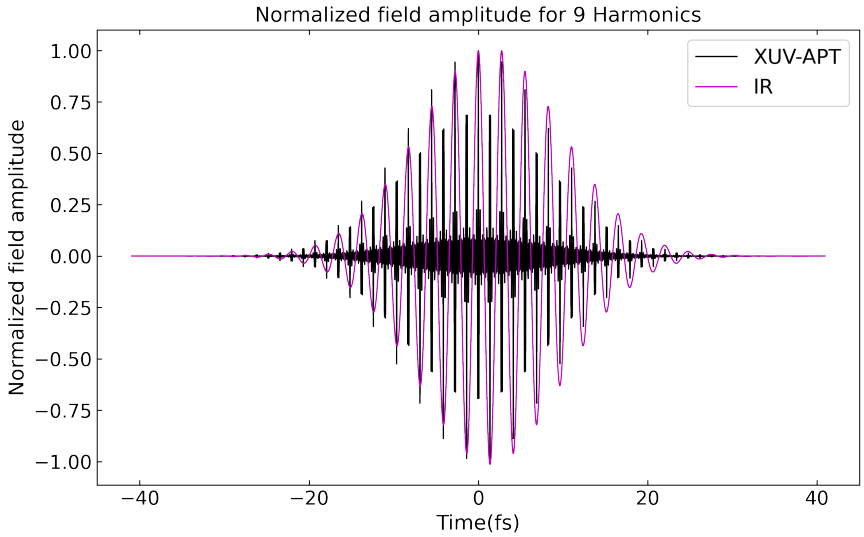

Figure 28: The normalized field amplitude as a function of time.

Photoionization by the XUV APT leads to harmonic peaks (black peaks), which can be clearly seen in Figure 28. The spectrum contains only odd harmonics, which are each at a distance of $2\omega_0$. There is a harmonic at 11, 13, 15, 17,..., 27 ω/ω_0. Figure 29 shows the XUV APT and IR pulse overlaid.

A closeup of figure 28 can be found in the appendix (A.6).

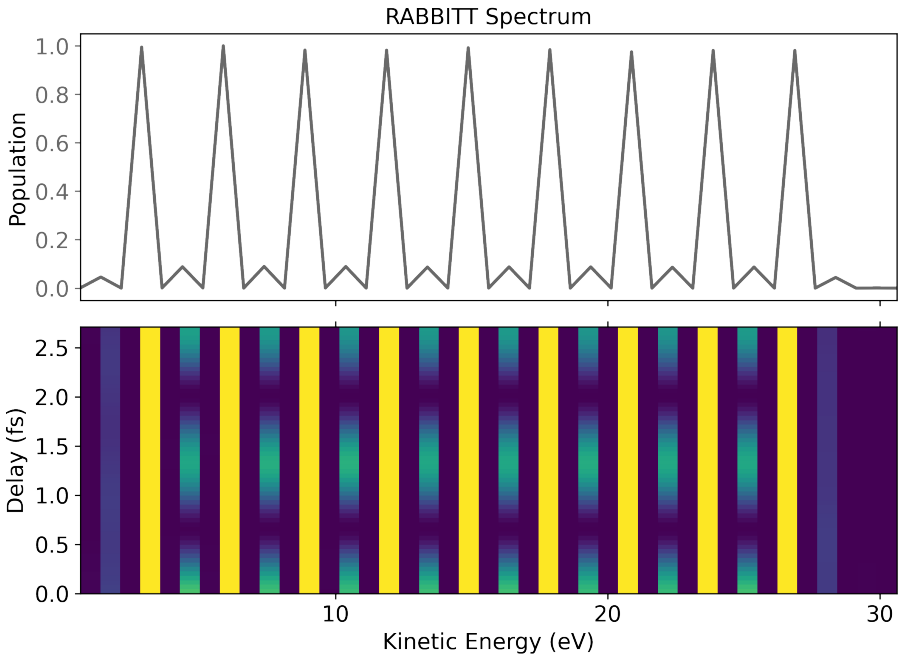

Figure 29: The RABBITT Spectrum: At the top is the population, where the major peaks are the harmonics and the peaks in between are the sidebands. Below is the contour plot of the associated 1-SB RABBITT spectrum.

At the top of the Figure, the population is plotted as a function of kinetic energy. You can see 9 major peaks and smaller peaks in between. The major peaks can be associated with the harmonics and the smaller peaks can be associated with the sidebands. The color bar below represents the delay-resolved pump-probe RABBITT scan, where the intensity oscillations are visualized in each of the sidebands. The intensity oscillations are the same for each sideband.

The population of the sidebands as a function of the delay is shown below, as well as the Fourier transformation of the harmonics oscillation:

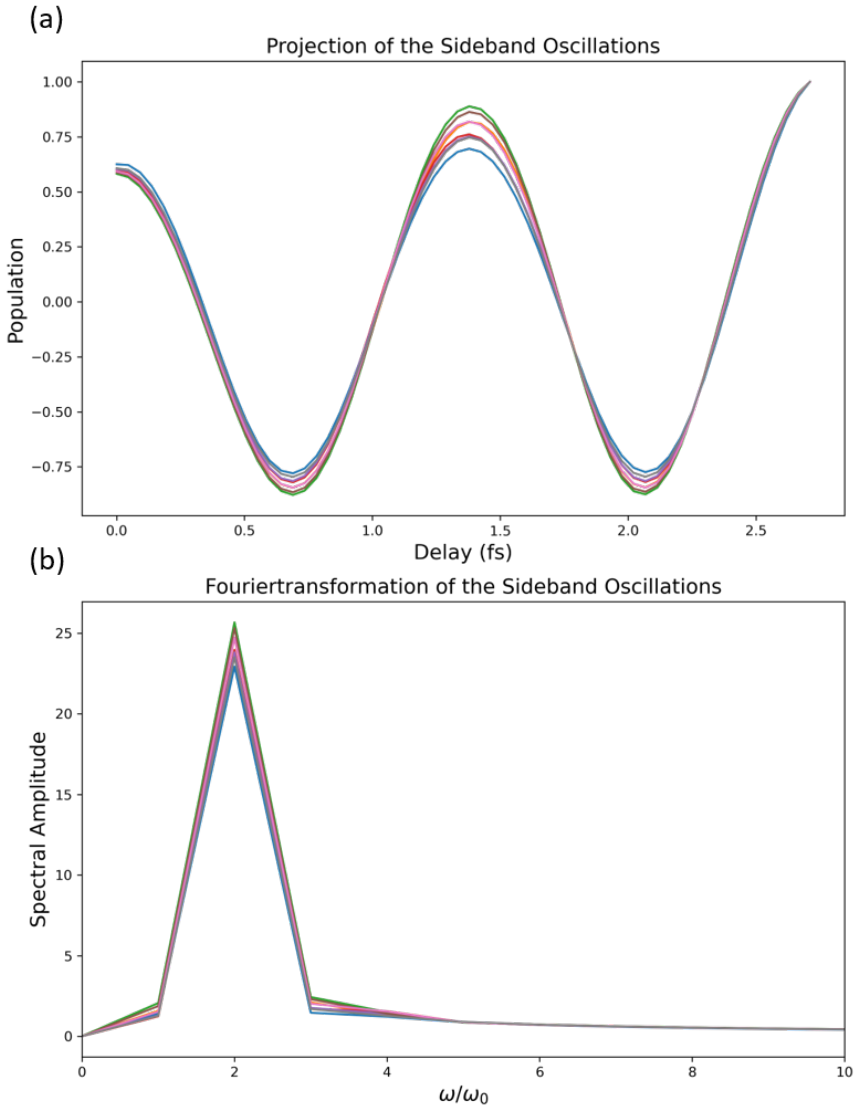

Figure 30: (a) the Population of the Sidebands as a function of the Delay and (b) the Fouriertransformation of the Sideband Oscillations as a function of the frequency.

The population of the sidebands hardly differs, regardless of the time delay. Small differences can be seen in the population peaks, but these are not significant. Furthermore, the sideband oscillation is Fourier transformed and plotted against the frequency. One recognizes that all sidebands have the same peak at $2\omega/\omega_0$ and thus one can conclude from Figure 30(b) that the sidebands all oscillate at the same frequency $2\omega_0$.

Furthermore, consider the oscillation of the sidebands and the harmonics. For this we fit a cosine function to the harmonic signal and to the sideband signal.

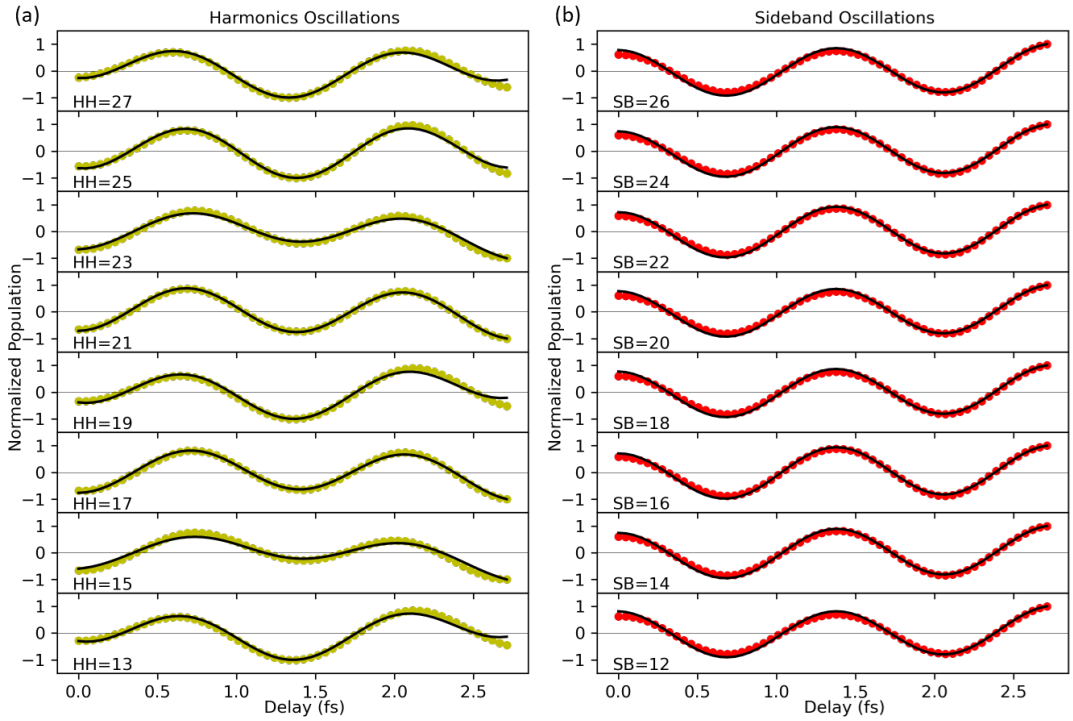

Figure 31: (a) fit of a cosine function to the harmonic signal and (b) fit of a cosine function to the sideband signal.

The figure 31 shows the normalized population, on the one hand (a) for the harmonics and on the other hand (b) for the sidebands, as well as the fits of the oscillations to the cosine function. As expected, the normalized population for 32(a) is shifted by π to (b), so that the harmonics and sidebands are always alternately populated and unpopulated with respect to each other.

The next figure shows the phase and the atomic time delay of the sideband oscillation:

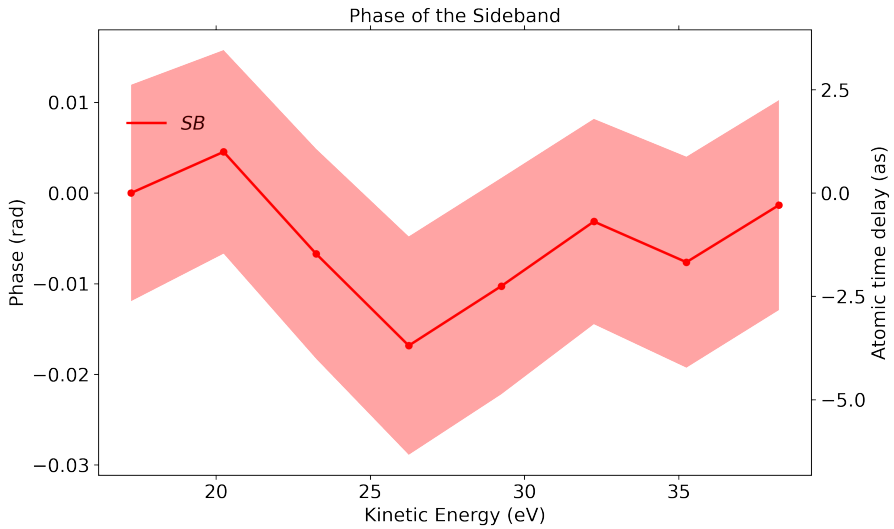

Figure 32: The retrieved Pahse of the Sideband oscillation.

In Figure 32 it can be seen that the phase alternately slightly decreases and increases with the kinetic energy. The phase as well as the atomic time delay of the sideband oscillation is close to zero since the XUV-pulse is not chirped.

5.2 RABBITT with phase shift of the XUV pulses

In the next section, as already announced above, we compare the RABBITT technique with and without a chirped XUV-pulse. The remaining information and conditions are the same as for section (5.1) above.

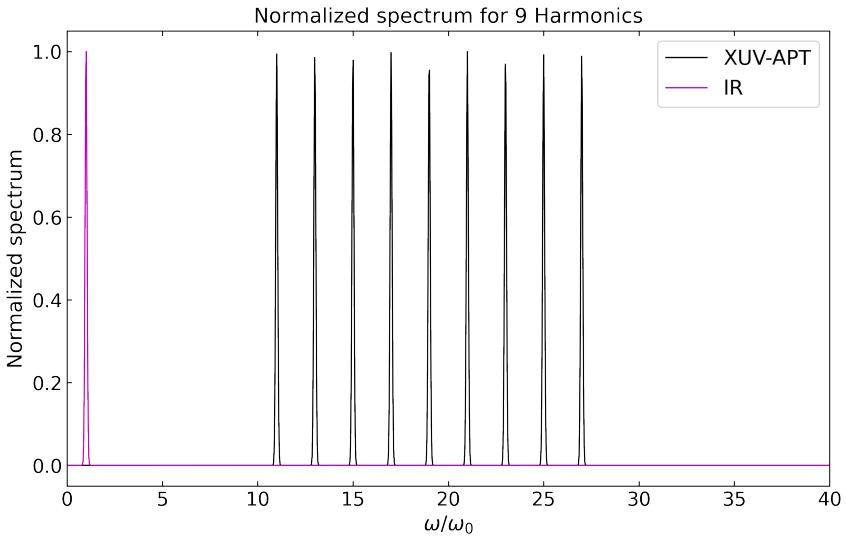

Figure 33: The normalized spectrum as a function of freequency. The 9 Harmonics (black peaks) are centered around $19\omega/\omega_0$ and are $2\omega/\omega_0$ apart from each other.

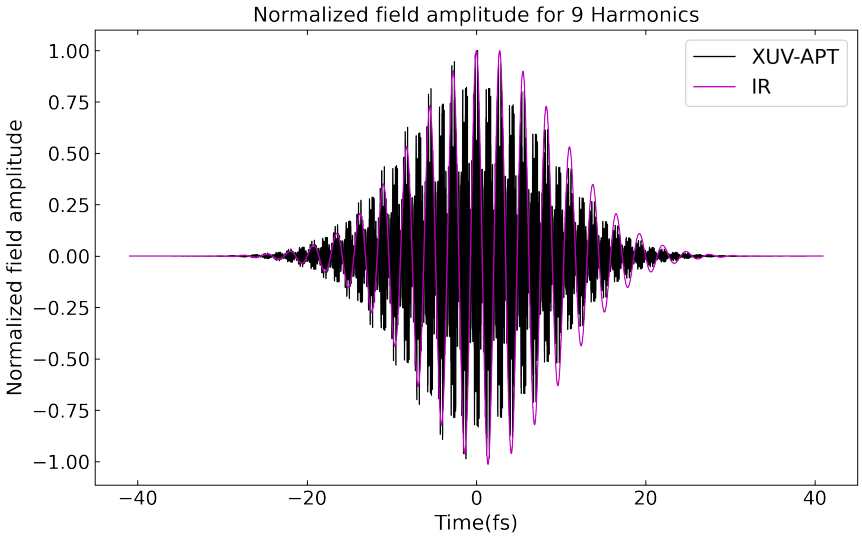

Figure 34: The normalized field amplitude as a function of time.

Figure 33 only shows the XUV APT again, i.e. the 9 harmonic peaks, but there is no difference to Figure 27. Due to the chirp, there is a difference in Figure 34 (in comparison to Fig. 28). The XUV APT are wider and not as precise as for $chirp = 0$.

The following figure shows at the top the Population as a function of the kinetic energy and below the contour plot of the 1-SB RABBITT spectrum.

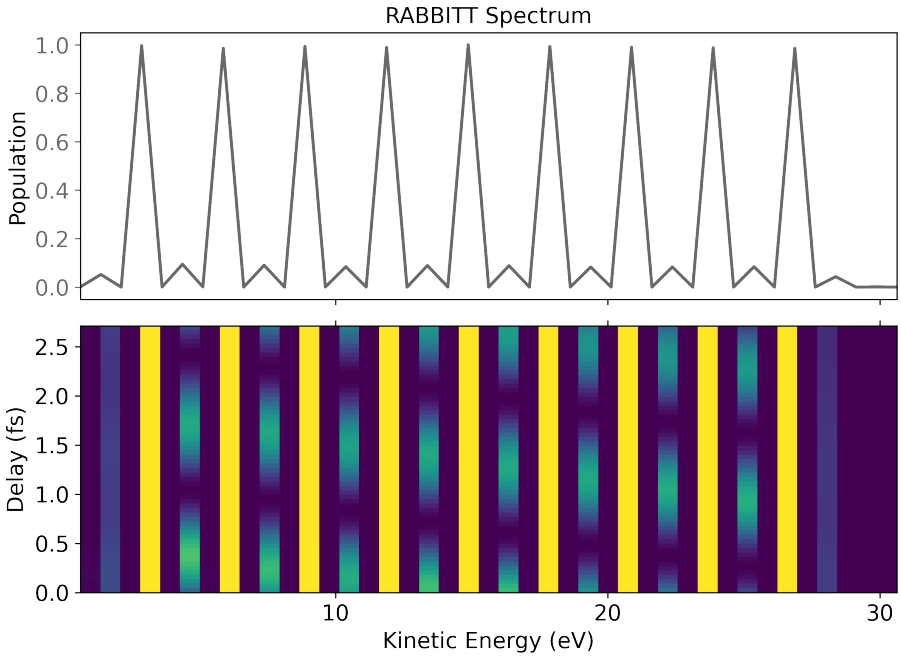

Figure 35: The RABBITT Spectrum: At the top is the population, where the major peaks are the harmonics and the peaks in between are the sidebands. Below is the contour plot of the associated 1-SB RABBITT spectrum.

The population probability remains the same as for $chirp = 0$, but in Figure 35 below you can see that the intensity oscillation shifts with the kinetic energy.

In figure 36(a) the population of the Sidebands is plotted as a function of the delay and in fig. 36(b) you can see the Fouriertransformation of the Harmonics Oscillation as a function of the frequency:

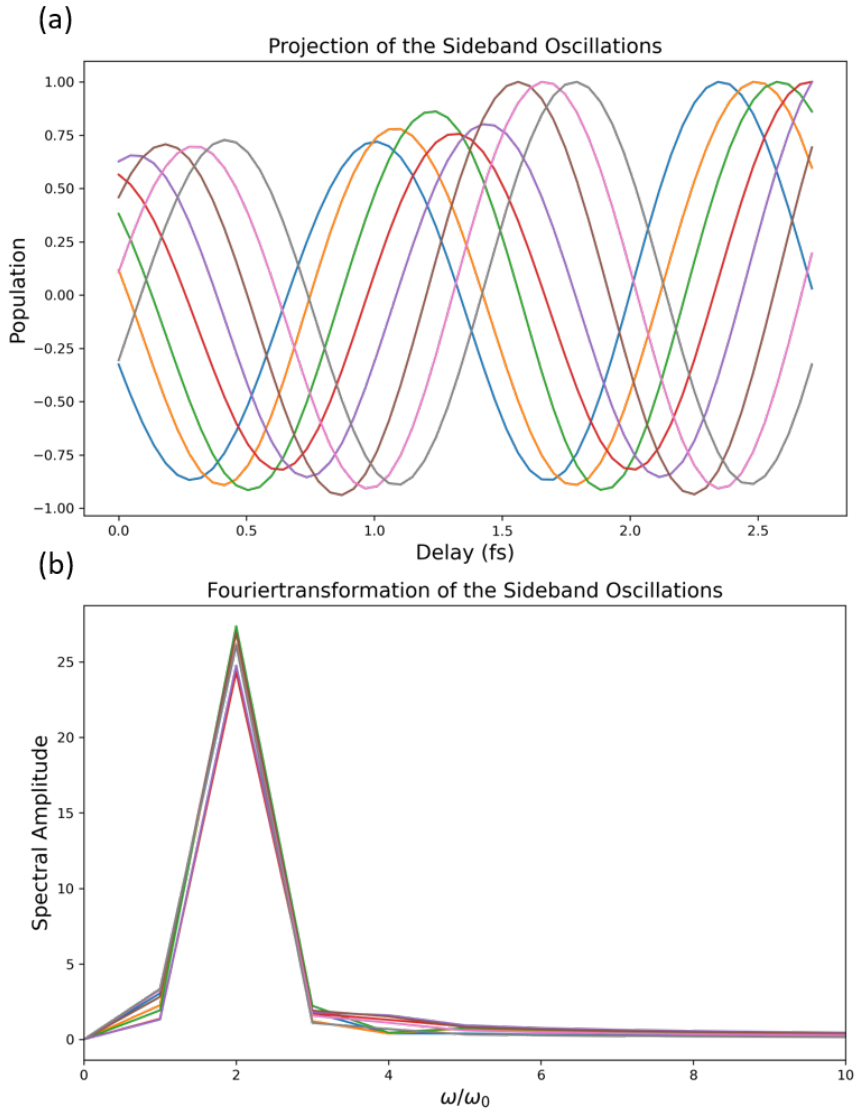

Figure 36: (a) the Population of the Sidebands as a function of the Delay and (b) the Fouriertransformation of the Sideband Oscillations as a function of the frequency.

Fig. 36b) hardly differs from the case $chirp = 0$ but in Fig. 36(a) one can see a significant difference in the population of the sidebands. The populations are all shifted by a similar or the same distance from each other.

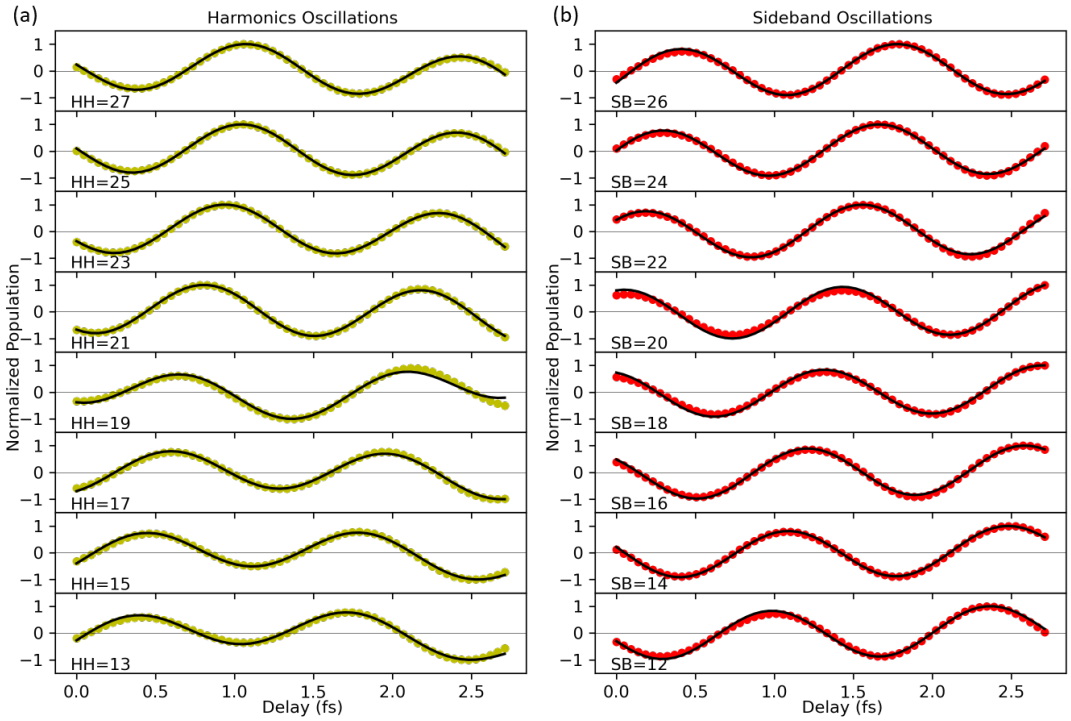

Figure 37: (a) fit of a cosine function to the harmonic signal and (b) fit of a cosine function to the sideband signal.

The normalized population for the harmonic oscillation as well as for the sideband oscillation, which is shown in Fig. 37, is shifted by about π compared to the case $chirp = 0$.

For the next figure one compares the representation of the phase and the atomic time delay of the sideband oscillation as a function of the kinetic energy, to the case $chirp = 0$.

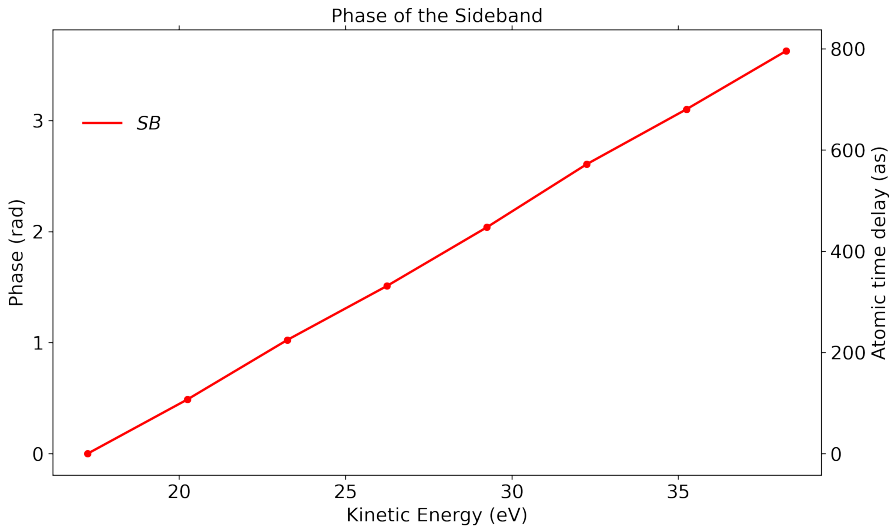

Figure 38: The retrieved Pahse of the Sideband oscillation.

In Fig. 38(a) the phase is not close to zero but increases linearly with increasing kinetic energy. That is the case, because of the chirped XUV-pulse, the intensity oscillation is shifted, which leads to a shift in the sideband oscillations and an increasing phase per kinetic energy.

In this chapter, the few-level model RABBITT was used to simulate and a comparison was made with a chirped XUV pulse and an XUV pulse with $chirp = 0$. From this it was possible to conclude that the intensity oscillation shifts as a result of the chirped pulse. This led to changes in the sideband oscillation and thus also in the phase. Although the sidebands oscillate with the same frequency $2\omega_0$, they are shifted in relation to one another, so that the phase increases linearly.

6 Conclusion

In this thesis the main goal was to test and simulate RABBITT with a Few-Level Model. For this, a very simple system was first used, namely the 2-level system. Then one continued with the 5-level system and finally, one applied the Few-Level Model to the 1-SB RABBITT technique.

At the beginning (chapter 2-level system) one considered 2 different methods for the interaction of a continuous electric field with a 2-level system in order to determine the equations of motion for the groundstate and the excited state and to be able to represent the population of the two energy levels: On the one hand, one uses the Rotating-Wave Approximation as an analytical method and the Runge-Kutta method as a numerical method. The two methods were finally compared and it turned out that the Rotating-Wave Approximation is only applicable to near-resonance cases, since the fast-rotating terms can no longer be neglected for a detunig $\Delta >> 0$. In the further course of the thesis, the Runge-Kutta method was continued. Then one continues to examine the interaction of a pulse with a 2-level system, varying the pulse area. One came to the result: For a 2π pulse the system is again in the initial state after the interaction, with a π pulse the system is in the excited state and at a $\pi/2$ pulse, the system is in a superposition of the ground state and the excited state. Furthermore, multiphoton transitions were examined, which turned out to be that an even number of photons is not absorbed, or the probability of this is very low. The probability of a transition also decreases, the larger the number of photons is: This means that a 1-photon absorption is more likely than a 3-photon absorption or a 5-photon absorption, etc. At the end of this chapter, a 2-Level System with decay was considered. Here it was distinguished between two cases: the decay of the excited state is added to the ground state or the population of the excited state decays but is not added to the ground state, instead ionization occurs. In the first case the total population remains constant 1 and in the second case the total population decreases over time.

In the next chapter the interaction on the one hand of with an continuous electric field and on the other hand with an pulse, which has a pulse area of 2π, with a 5-level system was considered. The photon energy is the same as for the 2-level system $E_{ph} = \omega \cdot \hbar/e = 1.5\ eV$. In addition, the distance between the energy levels was varied in both cases (ω, $\omega/2$, $\omega/4$) as well as the upper energy levels were densed (0.1ω, 0.01ω, 0.001ω). As expected, there were different representations of the occupation of the energy levels. Interestingly, for very closely spaced upper energy levels, the resonant energy level was no longer the most populated, instead the upper energy level populations were barely distinguishable. This was the case for an interaction with a continuous electric field and with a pulse of pulse range 2π.

In the last chapter, the few-level model RABBITT was used to simulate and a comparison was made with a chirped XUV pulse and an XUV pulse with $chirp = 0$. From this it was possible to conclude that the intensity oscillation shifts as a result of the chirped pulse. This led to changes in the sideband oscillation and thus also in the phase. Although the sidebands oscillate with the same frequency $2\omega_0$, they are shifted in relation to one another, so that the phase increases linearly. One considered a pump pulse containing nine odd harmonics (3,5,7,9,...,19) and accordingly eight even sidebands (4,6,8,...,18). The distance between the energy levels is $\omega_0 = 1.5/2\ \text{eV} \cdot e/\hbar$.

A further procedure could still be: To add a constant decay to the upper states (simular as for the 2-Level System with decay) or to add more numberof closely spaced energy levels near the resonance states (as for the 5-Level System) to approximate the high energy states to continuum states for RABBITT. It would also be interesting to examine the many oscillations that occur in the 5-level system.

A Appendix

A.1 2-Level System with Rotating-Wave Approximation

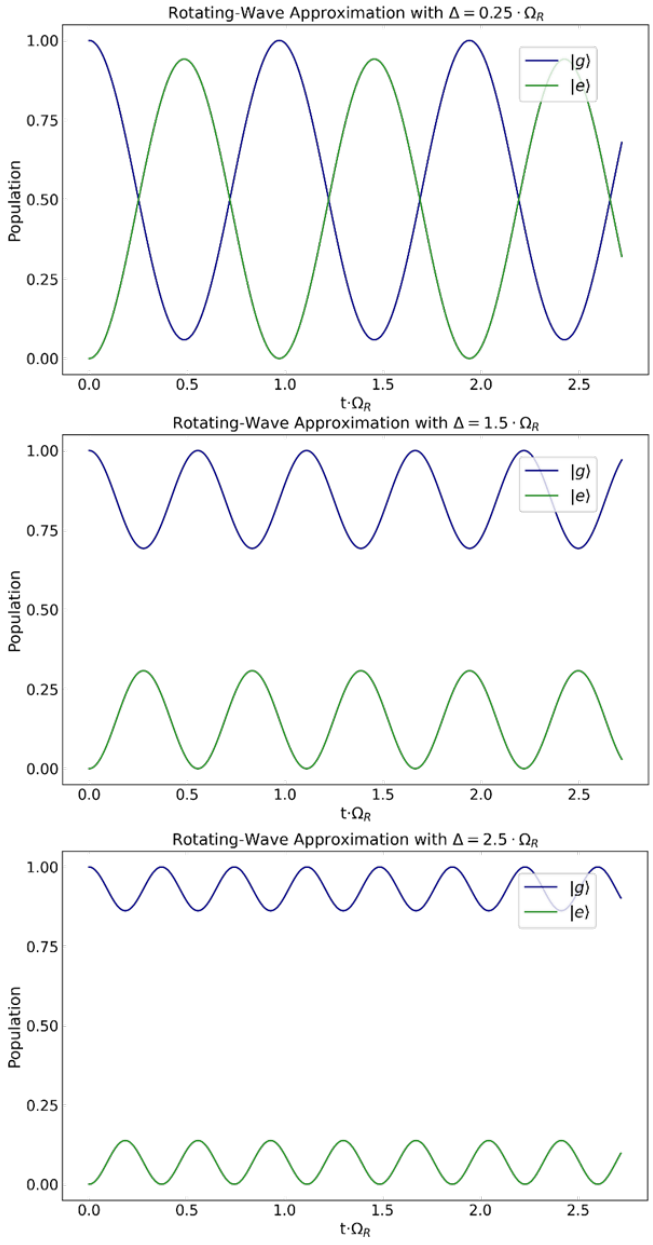

Figure 39: The Population of the ground state $|g\rangle$ and the upper state $|e\rangle$ (computed with the Rotating-Wave Approximation) at different detunings Δ.

A.2 2-Level System with Runge-Kutta Method

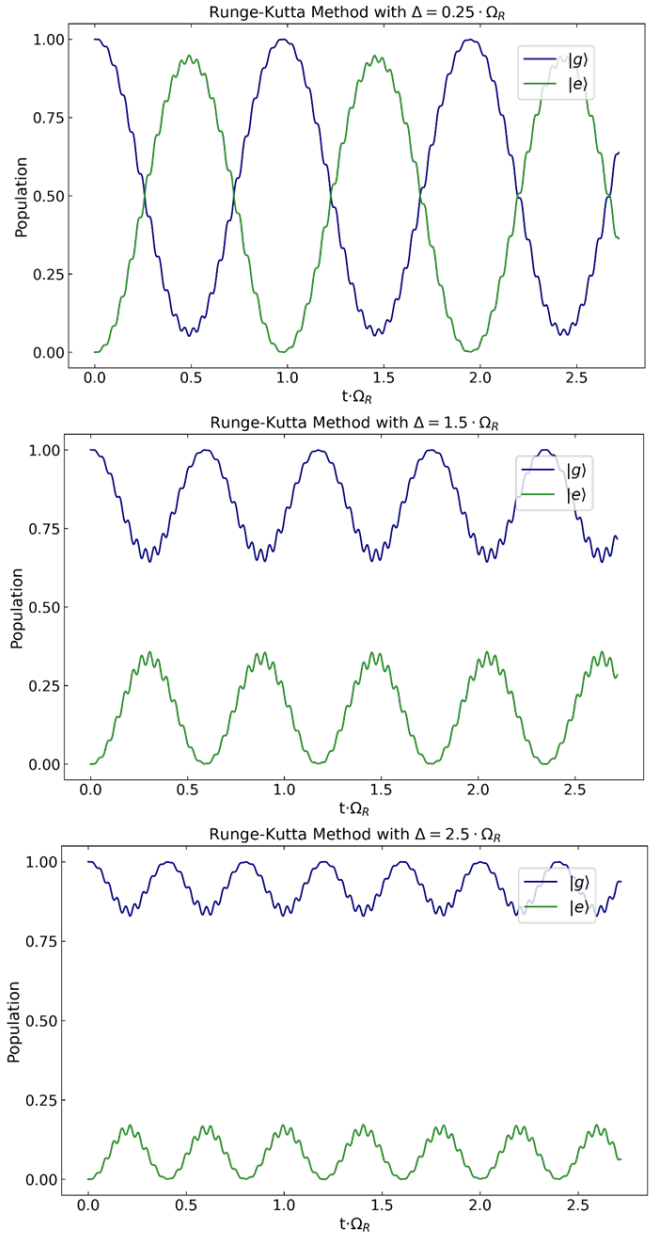

Figure 40: The Population of the ground state $|g\rangle$ and the upper state $|e\rangle$ (computed with the Runge-Kutta Method) at different detunings Δ.

A.2.1 2-Level System with Runge-Kutta Method and increasing the resonance frequency

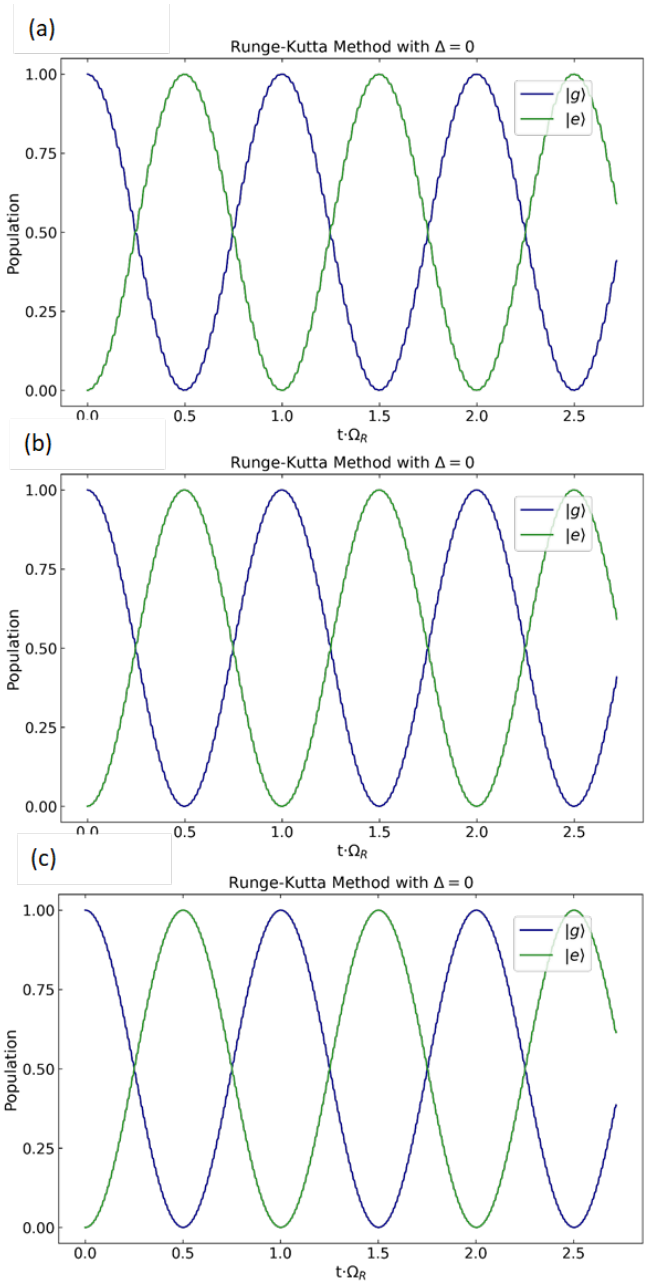

Figure 41: The Population of the ground state $|g\rangle$ and the upper state $|e\rangle$ (computed with the Runge-Kutta Method) with $\Delta = 0$ for different values for ω_0 ($\omega_0 = \omega_{eg}$). For (a) applies $2 \cdot \omega_0$, for (b) $3 \cdot \omega_0$ and for (c) applies $4 \cdot \omega_0$.

A.3 Pulsed Rabi oscillation in a 2-Level System

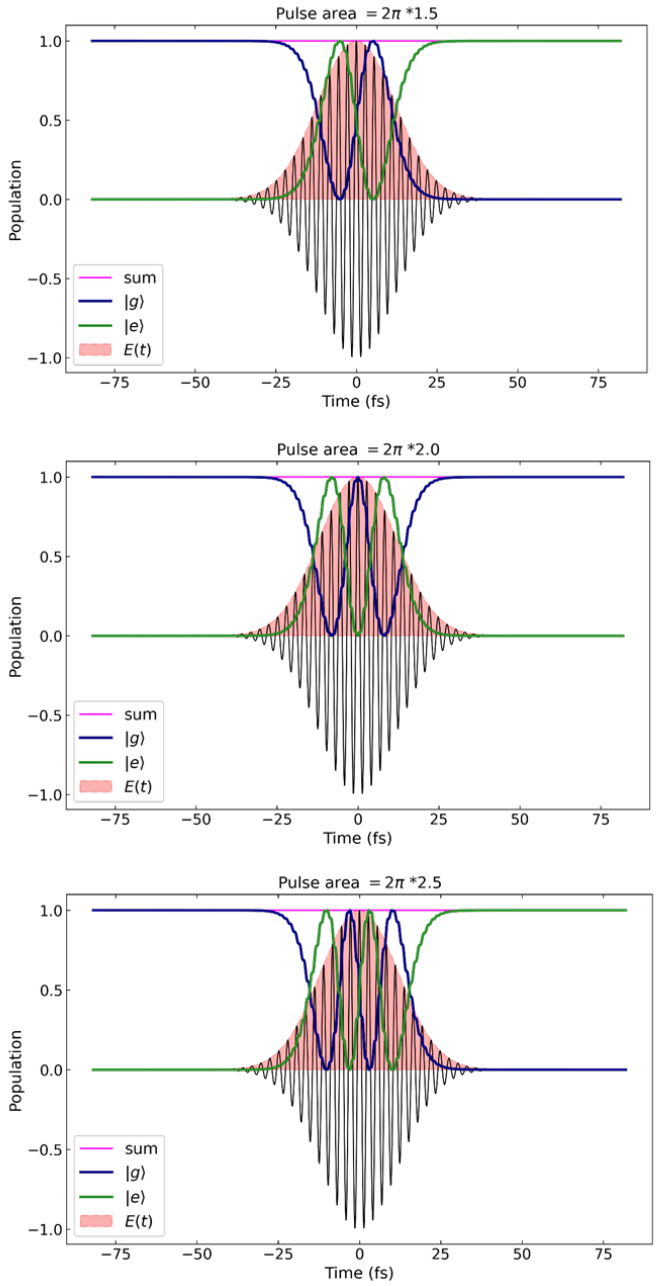

Figure 42: The Population of the ground state $|g\rangle$ and the upper state $|e\rangle$ after an interaction with an pulse. The pulse area is varied.

A.4 2-Level System with Decay

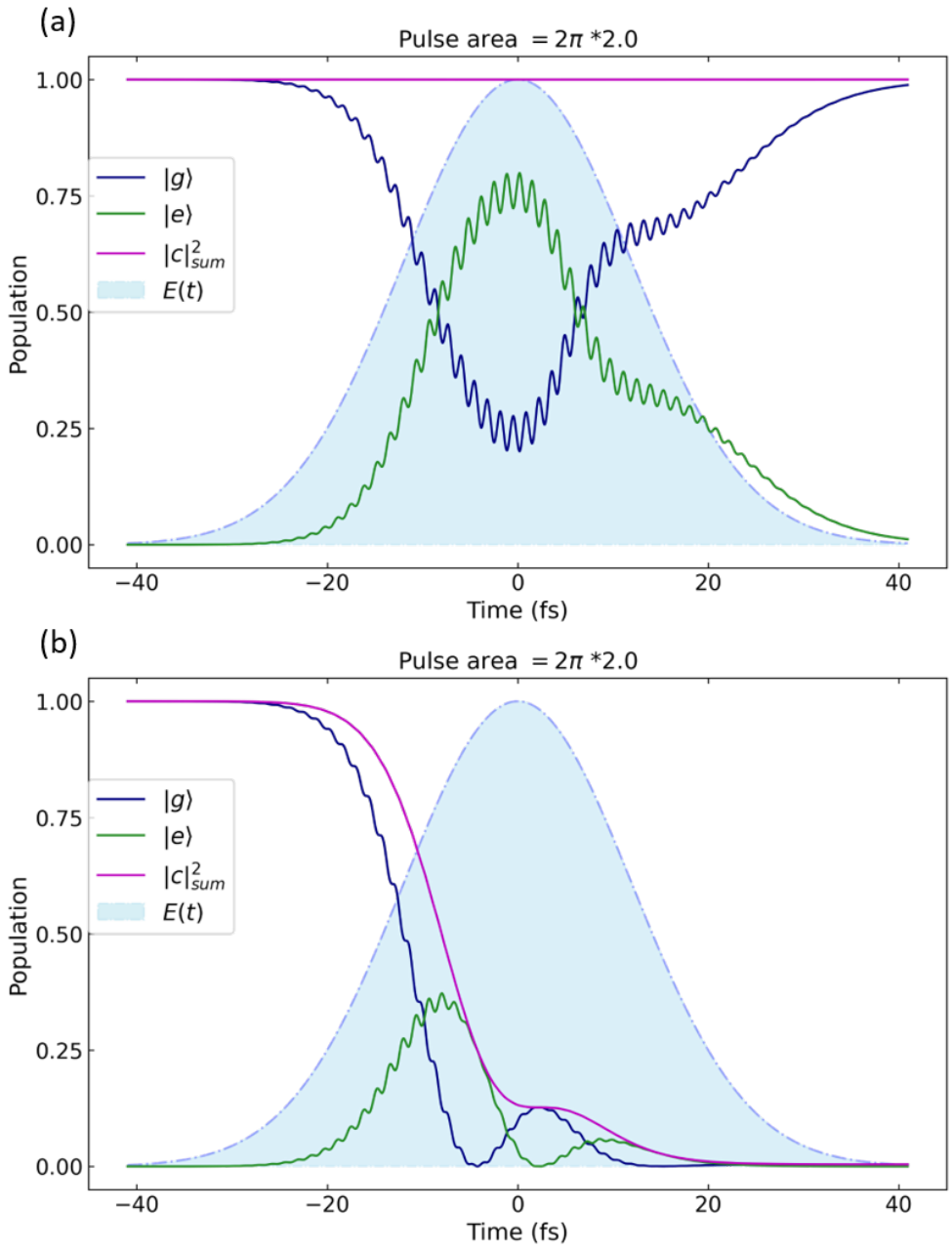

Figure 43: The Population of the ground state and the upper state, after an interaction with an pulse of Pulse Area 4π. In this case applies $0.25 \cdot \gamma$. For (a) the decay of the excited state is added to the ground state and for (b) the Population of the excited state decreases because of ionisation.

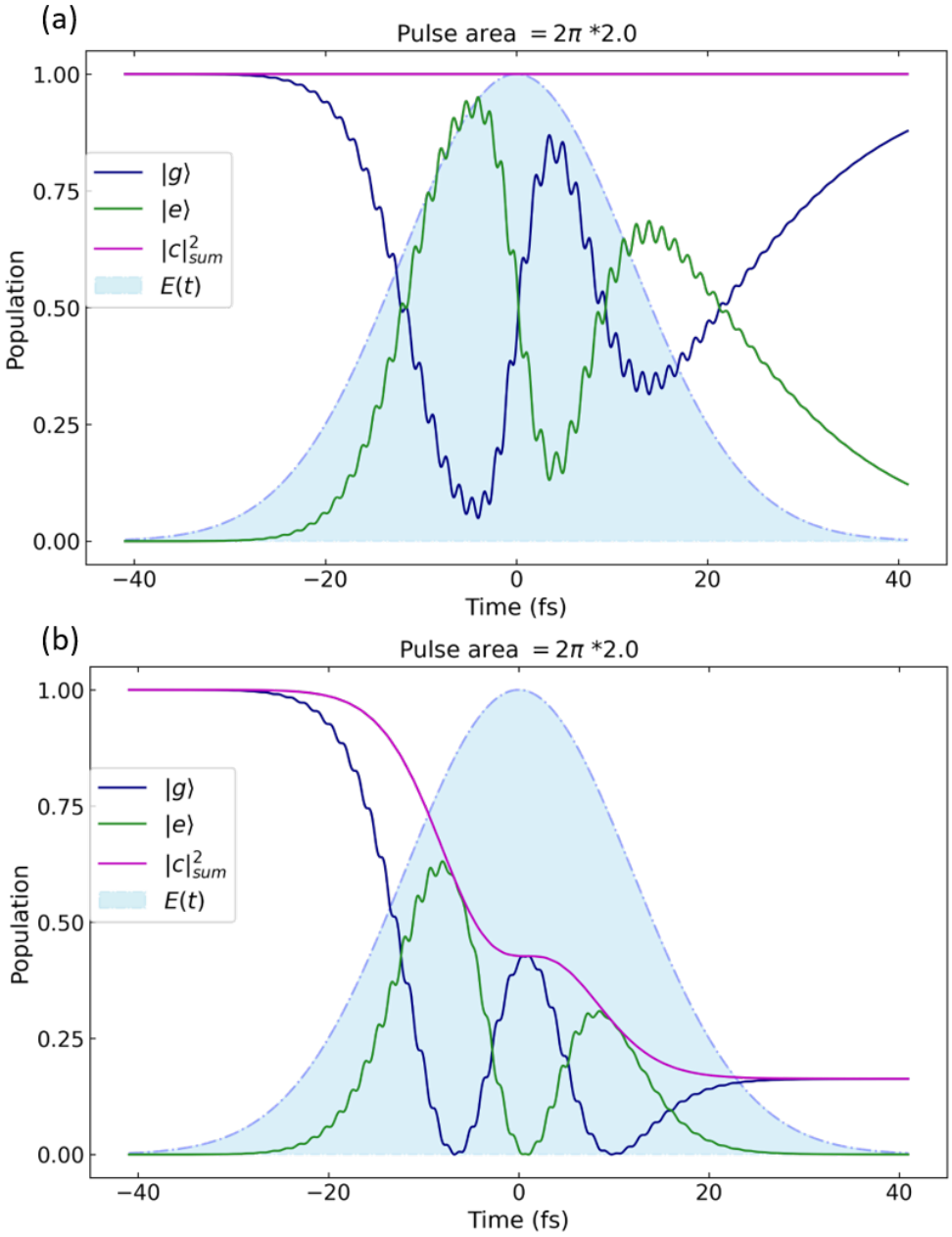

Figure 44: The Population of the ground state and the upper state, after an interaction with an pulse of Pulse Area 4π. In this case applies $10^{-1} \cdot \gamma$. For (a) the decay of the excited state is added to the ground state and for (b) the Population of the excited state decreases because of ionisation.

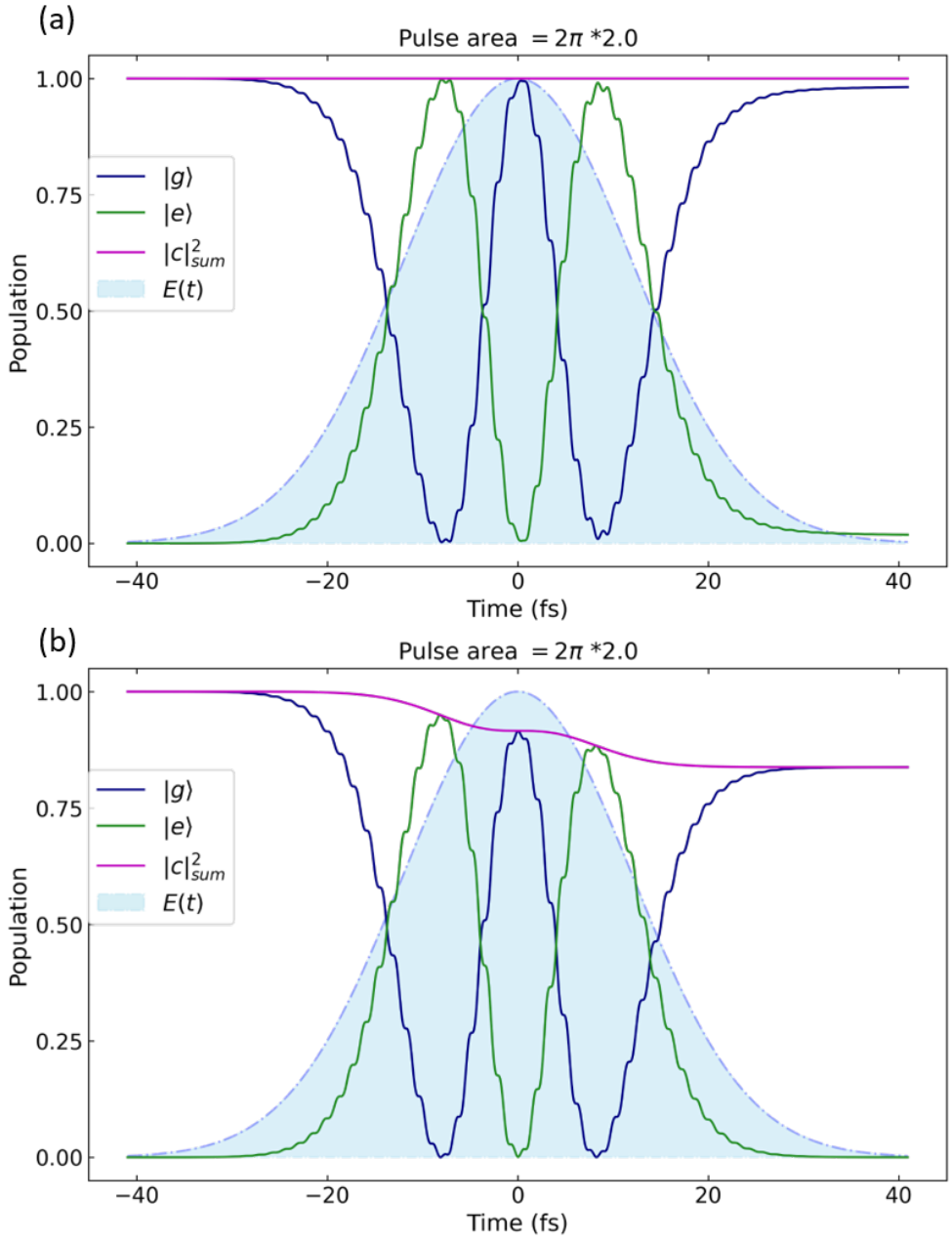

Figure 45: The Population of the ground state and the upper state, after an interaction with an pulse of Pulse Area 4π. In this case applies $10^{-2} \cdot \gamma$. For (a) the decay of the excited state is added to the ground state and for (b) the Population of the excited state decreases because of ionisation.

A.5 RABBITT

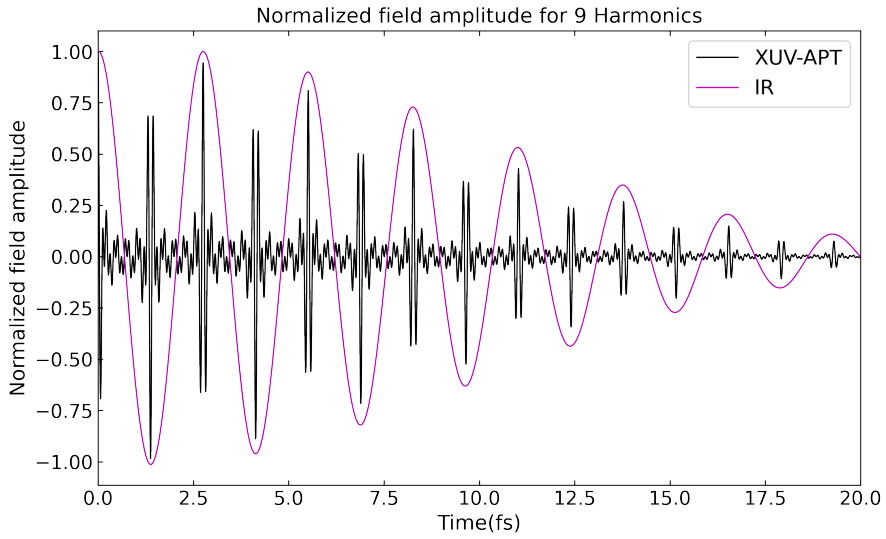

Figure 46: The normalized field amplitude as a function of time as a closeup.

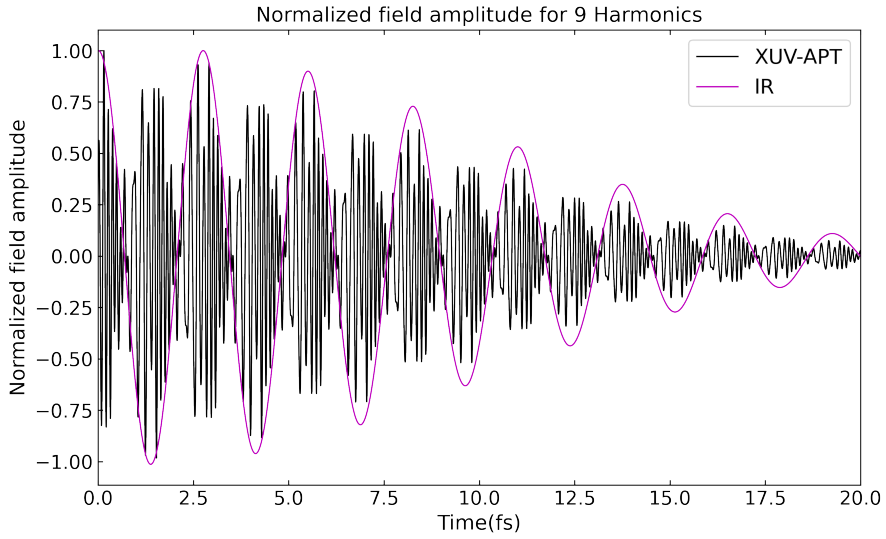

Figure 47: The normalized field amplitude as a function of time as a closeup and with a chirped XUV-pulse.

References

[1] J. Diels, W. Rudolph, P. Liao, and P. Kelley, *Ultrashort Laser Pulse Phenomena*. Optics and photonics, Elsevier Science, 2006.

[2] F. W. Cummings *Stimulated emission of radiation in a single mode*, Phys. Rev. 140(4A), 1051–1056 (1965).

[3] E. T. Jaynes and F. W. Cummings, *Comparison of quantum and semiclassical radiation theories with application to beam maser*, Proc. IEEE 51(1), 89–109 (1963).

[4] M. Tavis and F. W. Cummings, *Approximate solutions for an n-molecule-radiation-field hamiltonian*, Phys. Rev. 188(2), 692–695 (1969).

[5] T. V. Foerster, *Comparison of quantum and semiclassical theories of interaction between a 2-level atom and radiation-field*, J. Phys. Math. Gen. 8(1), 95–102 (1975).

[6] Saifullah, *Feedback control of probability amplitudes for two-level atom in optical field*, Opt. Commun. 281(4), 640–643 (2008).

[7] S. V. Prants and V. Y. Sirotkin, *Effects of the Rabi oscillations on the atomic motion in a standing-wave cavity*, Phys. Rev. A 64(3), 033412 (2001).

[8] V. Y. Sirotkin and S. V. Prants, *Random walking of a two-level atom in a standing-wave field*, Proc. SPIE 4750, 97–103 (2002).

[9] A. J. Leggett, S. Chakravarty, A. T. Dorsey, M. P. A. Fisher, A. Garg, and W. Zwerger, *Dynamics of the dissipative 2-state system*, Rev. Mod. Phys. 59(1), 1–85 (1987).

[10] S. Borisenok and S. Khalid, *Linear Feed forward Control of Two-Level Quantum System by Modulated External Field*, Opt. Commun. 284(14), 3562–3567 (2011).

[11] S. Khalid, *Two-Level Decay Quantum System with Open-Loop Control Optical Field*, J. Opt. Soc. Am. B 30(2), 428–430 (2013).

[12] C. C. Chang and L. Lin, *Light-mediated quantum phase transition and manipulations of the quantum states of arrayed two-level atoms*, New J. Phys. 14(7), 073018 (2012).

[13] B. W. Shore and P. L. Knight, *The Jaynes-Cummings model*, J. Mod. Opt. 40(7), 1195–1238 (1993).

[14] M. D. Crisp, *Application of the displaced oscillator basis in quantum optics*, Phys. Rev. A 46(7), 4138–4149 (1992).

[15] J. Gea-Banacloche, *Jaynes-Cummings model with quasiclassical fields - the effect of dissipation*, Phys. Rev. A 47(3), 2221–2234 (1993).

[16] W. H. Steeb, N. Euler, and P. Mulser, *Semiclassical Jaynes-Cummings model, painleve test, and exact-solutions*, J. Math. Phys. 32(12), 3405–3406 (1991).

[17] M. Jelenska-Kuklinska and M. Kus, *Resonance overlap in the semiclassical Jaynes-Cummings model*, Quantum Opt. 5(1), 25–31 (1993).

[18] B. W. Shore, *Coherent manipulations of atoms using laser light*, Acta Phys. Slovaca 58(3), 243–486 (2008).

[19] W. H. Louisell, *Quantum Statistical Properties of Radiation* (John Wiley Sons, 1973).

[20] M. Sargent III, M. O. Scully and W. E. Lamb, Jr., *Laser Physics* (Addison-Wesley, 1974).

[21] G. W. Ford and R. F. O. O'Connell, *The rotating wave approximation (RWA) of quantum optics: serious defect*, Physica A 243(3–4), 377–381 (1997).

[22] J. Seke, *Spontaneous emission of a 2-level system and the influence of the rotating-wave approximation on the final-state*, J. Stat. Phys. 33(1), 223–229 (1983).

[23] I. Schek, M. L. Sage, and J. Jortner, "Validity of the rotating wave approximation for high-order molecular multi-photon processes," Chem. Phys. Lett. 63(2), 230–235 (1979).

[24] Y. Wu and X. X. Yang, *Strong-coupling theory of periodically driven two-level systems*, Phys. Rev. Lett. 98(1), 013601 (2007).

[25] I. I. Rabi, *Space quantization in a gyrating magnetic field*, Phys. Rev. 51(8), 652–654 (1937).

[26] Y. Kaluzny, P. Goy, M. Gross, J. M. Raimond, and S. Haroche, *Observation of self-induced Rabi oscillations in 2-level atoms excited inside a resonant cavity - the ringing regime of superradiance*, Phys. Rev. Lett. 51(13), 1175–1178 (1983).

[27] M. Opher-Lipson, E. Cohen, A. Armitage, M. S. Skolnick, T. A. Fisher, and J. S. Roberts, *Magnetic field effect on the Rabi-split modes in GaAs microcavities*, Phys. Status Solidi A 164(1), 35–38 (1997).

[28] I. Tittonen, M. Lippmaa, E. Ikonen, J. Lindén, and T. Katila, *Observation of mössbauer resonance line splitting caused by Rabi oscillations*, Phys. Rev. Lett. 69(19), 2815–2818 (1992).

[29] U. Herzog and J. A. Bergou, *Reflection of the Jaynes-Cummings dynamics in the spectrum of a regularly pumped micromaser*, Phys. Rev. A 55(2), 1385–1390 (1997).

[30] I. Tittonen, M. Lippmaa, E. Ikonen, J. Lindén, and T. Katila, *Observation of mössbauer resonance line splitting caused by Rabi oscillations*, Phys. Rev. Lett. 69(19), 2815–2818 (1992).

Danksagung

Das Wichtigste in dieser Arbeit ist es sich bei allen zu bedanken, die mich während der Zeit unterstützt haben.

An erster Stelle bedanke ich mich herzlich bei **Robert Moshammer**, der es mir ermöglicht hat, die Arbeit in seiner Abteilung zu schreiben und Ein herzliches Dankeschön gebührt **Thomas Pfeifer**, der so freundlich war und die Zweitkorrektur übernommen hat.

Mein größter Dank gilt aber **Anne Harth** und **Divya Bharti**. Ihr habt mich betreut und wart immer jeder Zeit für neue Fragen und für Diskussionen neuer Ergebnisse für mich da.

Zu guter Letzt gilt mein Dank an meine Freunde, meinen Eltern und meinen Geschwistern, **Signe und Simon**, die immer hinter mir standen und mich auf meinem Weg begleitet haben.